Collective directional memory controls the range of epithelial cell migration

Helena Canever[a,*], Hugo Lachuer[a,*], Quentin Delaunay[a], François Sipieter[a], Nicolas Audugé[a], Philippe P. Girard[a], and Nicolas Borghi[a]

[a]Université de Paris, CNRS, Institut Jacques Monod, 75013 Paris, France
[*]These authors contributed equally

Cell migration is a fundamental behavior involved in multicellular development, regeneration, and homeostasis, which is deregulated in cancer. Epithelial cells migrate individually when isolated and collectively within a tissue. However, how interactions between cells affect their ability to explore space and their sensitivity to guidance signals is poorly understood. Here, we show that isolated cells that are persistent random walkers adopt a superdiffusive behavior in an epithelium. The effect is stronger than external guidance cues and enables cells to reach greater distances than when isolated. This directional memory emerges from fractional Brownian motion that relies on velocity coordination between neighboring cells with intact cytoskeletal connections to intercellular adhesion complexes. Furthermore, we show how the stability and mechanosensitivity of adhesion complexes ultimately regulate the speed of collective migration and the sensitivity to guidance signals via dimerization of the adhesion protein vinculin. Together, our results show how cell speed, persistence, and directionality define the efficiency of spatial cell exploration on short, intermediate, and long time scales, respectively.

Cell migration | Epithelium | Cell adhesion
Correspondence: ***nicolas.borghi@ijm.fr***

Introduction

In multicellular organisms, cell migration is an essential process in tissue morphogenesis, homeostasis, and repair. Deregulation of cell migration is also involved in the metastatic invasion of cancers (1). Cell migration occurs in different ways, depending on the intrinsic properties of cells and how they interact with each other and their environment. As a result, cells may migrate individually or collectively, guided by local or global signals (2).

For these reasons, how cells explore their environment and how cell interactions and guidance cues affect this exploration are fundamental questions that have motivated abundant research for over 70 years (3, 4). Since then, various models have proven useful in describing the exploration of space by individually migrating cells. Directional persistence has emerged as a consistent, though highly variable, feature depending on the type of cell or the context, and could arise from the non-Gaussian distribution of cell displacements, temporal velocity correlations, or both (5–8). When migrating collectively, neighbor cells typically exhibit correlated velocities that depend on their interactions (9–11). This coordination and the diverse mechanisms underlying it have been the subject of intense scrutiny for the past decade (12). In comparison, how each cell in the collective explores its environment has received much less attention, with a few exceptions (13–15). Remarkably, it remains unclear whether neighbor interactions actually help or hinder the exploratory capacity or sensitivity to guidance cues of each cell in the collective, much less whether and how they quantitatively or qualitatively affect the underlying cellular and molecular mechanisms of migration.

Adherent cells form Focal Adhesions (FAs) on their substrate, which they continuously assemble at their front and dissassemble at their back during migration (16). There, mechanosensory proteins, such as vinculin, provide force transmission from the contractile cytoskeleton (17). In cohesive tissues, cells also adhere to each other through cadherin-based Adherens Junctions (AJs) where α-catenin and vinculin enable dynamic connections with the cytoskeleton and force transmission (18). Vinculin comprises a head and a tail domain whose intramolecular interaction competes with intermolecular dimerization and binding to the actin cytoskeleton of its tail and with binding of its head to adapter proteins in FAs and AJs (19). In AJs, α-catenin is this adapter, which also binds actin by its own tail (20). Vinculin deficiencies impact the migration of cells as individuals, in a collective and with guidance cues, although in a cell type- and mutation-dependent manner (11, 21–32). Alpha-catenin deficiencies have an impact on guided and coordinated collective migration, involving the interaction of α-catenin with vinculin in AJs (11, 26, 33, 34). However, the lack of comparable metrics, scales and molecular, cellular and migratory contexts between studies makes it difficult for a general picture to emerge, where the functions of proteins in regulating the stability and mechanosensitivity of adhesions could explain how they control the intrinsic speed of cells, their persistence, and their responses to interactions with neighbors and guidance cues.

Here, we address this issue by comparing the exploratory ability of epithelial cells as individuals, in the collective and exposed to a guidance cue, while genetically disrupting the interactions of cells with their substrate and neighbors and monitoring the associated effects on the dynamics and mechanics of adhesion complexes. We show that individual epithelial cells migrate with transient directional memory and that vinculin regulates their speed by synergizing FA stability and cytoskeletal tension transmission through its dimerization and actin-binding abilities, respectively. In contrast, cells that migrate collectively acquire virtually infinite di-

rectional memory, which specifically requires α-catenin in AJs and results from the coordination of velocities between neighboring cells. In this context, vinculin additionally controls the speed of cells from their AJs through its impact on their mobility and force transmission, but in a manner specifically dependent on its dimerization. Overall, this results in a spatial exploration that is less efficient than that of individual cells on time scales less than $\sim$ 3hrs but more efficient beyond that. Finally, cell guidance by an epithelial wound also requires α-catenin, but the directional bias is too small to significantly affect the efficiency of spatial exploration for hours. In this context of guided collective cell migration, vinculin dimerization further regulates cell speed from AJs by providing mechanosensitivity to the entire epithelium of the wound.

Results

Single epithelial cells are persistent random walkers. To characterize the motion of single epithelial cells, we tracked nucleus-stained MDCK cells overnight, sparsely plated on collagen-coated glass coverslips (see Materials and Methods)(Fig. 1A, movie 1). We found that a persistent random walk model (35, 36) was more likely than a pure or superdiffusion model to describe the average Mean Square Displacement (MSD) as function of time interval Δt: the MSD transitioned from ballistic (slope 2 for small Δt in ln-ln scale) to pure diffusion (slope 1 for large Δt) with a persistence time of the order of 10min (Fig. 1B; Table S1). To confirm the underlying walk model, we examined the step size R for the time intervals $\Delta t = 10$min and $\Delta t = 3$hrs. In both cases, R followed a Rayleigh distribution, in agreement with a Gaussian walk regardless of temporal resolution (Fig. 1C, S1A). Finally, we examined the angular memory, which we define as the deviation of each elementary 10min step from the past direction over an increasingly longer past (Δt, see Materials and Methods). We found that its distribution was skewed towards small angles at small Δt and uniform at large Δt (Fig. S1B). In other words, the angular memory decreased with increasing Δt (Fig. 1D). Overall, these results show that single epithelial cells migrate as persistent random walkers, displaying transient directional persistence overcome by pure diffusion on longer time scales.

To investigate the robustness of this behavior, we examined the effects of overexpressing full-length (FL) vinculin or vinculin mutants, additionally bearing a tension sensor module (37, 38). Specifically, we considered the Tailless mutant (TL) that impairs all tail interactions (39), the T12 mutant that impairs the head-tail interaction (40) and the Y1065E (YE) mutant that impairs the tail-tail interaction (41) (Fig. S2A). All stable cell lines (Fig. S2B,C) exhibited an MSD better described by a persistent random walk model than by a pure or superdiffusion model (Fig. 2A, Table S1). The effects of mutant expression on persistence times and diffusion coefficients were variable and did not show a correlation (Fig. S2D). In addition, the diffusion coefficient scaled well with the squared apparent speed with a common persistence time for all cell lines (Fig. S2E), showing that cell lines differed primarily in apparent speed rather than persistence. Specifically, TL and YE mutants with impaired actin-tail or tail-tail interactions decreased cell speed, while the T12 mutant with altered head-tail interaction increased cell speed relative to FL vinculin (Fig. 2B). This could not be explained by differences in expression levels between cell lines since the effects of YE and TL were stronger than those of FL despite an equal or lower expression, and those of T12 completely opposite despite a higher expression (Fig. S2F). Rather, this indicated a dominant effect, consistent with previous reports (39). Overall, these results show that the persistence, but not the speed of single migrating cells is robust to mutations in the FA protein vinculin.

The combination of Focal Adhesion stability and force transmission from the cytoskeleton predicts the migration speed of single cells. The transmission of cytoskeletal forces through FAs is essentially based on vinculin (39, 42, 43). Thus, to identify the underlying cellular mechanisms and molecular determinants of speed regulation by FAs, we took advantage of the tension sensor module in vinculin and its mutants to assess their mechanical state by Molecular Tension Microscopy (Fig. 2C) (see Materials and Methods). We found that alteration of actin-tail and head-tail interactions (TL and T12) decreased and increased vinculin tension relative to FL vinculin, respectively (Fig. 2D), as seen in other cell types (37, 38). In contrast, alteration of the tail-tail interaction (YE) did not substantially affect vinculin tension, meaning that vinculin dimerization is unnecessary for force transmission (Fig. 2D). Next, we investigated a potential relationship between vinculin tension and single cell speed across mutants, but found no significant correlation (Fig. S2G), indicating that single cell speed is not simply a result of vinculin force transmission.

The stability of the core cytoskeletal linkers of FAs is based on vinculin (30, 44). Therefore, we investigated the effects of mutations on vinculin turnover by Fluorescence Recovery After Photobleaching (FRAP, Fig. S2H, movie 2) (see Materials and Methods). We found that TL and T12 mutants, both of which impair head-tail interaction, had a significantly higher immobile fraction than FL vinculin (Fig. 2E), consistent with previous studies in other cell types (30, 39, 44–47). This shows that impaired head-tail interaction, regardless of tension, is sufficient for vinculin stability. Conversely, the YE mutant that impairs the tail-tail interaction showed a significantly smaller immobile fraction (Fig. 2E). This shows that vinculin dimerization promotes its stability. Additionally, this shows that cell migration speed does not simply result from vinculin stability since T12 and TL induce opposite effects on migration speed while both stabilize vinculin, and T12 and YE have antagonist effects on vinculin stability while both promote cell speed.

Together, this supports that migration speed decreases upon loss of force transmission or FA stability (TL and YE) and increases upon strengthening of both (T12). We therefore propose that single cell migration speed is the product of FA stability and force transmission, the former enabled by vinculin tail-tail interaction and the latter by vinculin-actin binding,

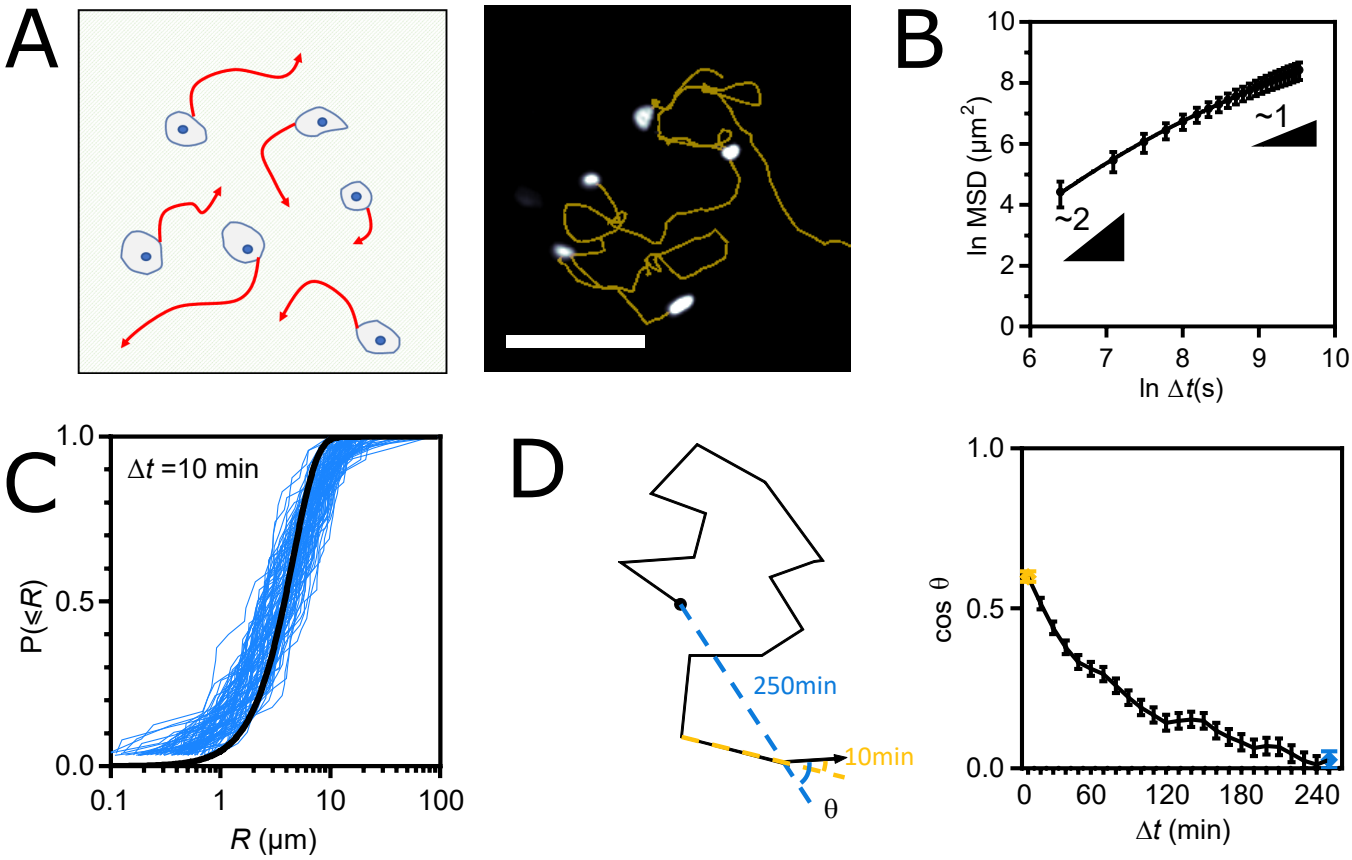

Fig. 1. (A) Left: Schematic representation of the single cell migration assay. Right: fluorescence image of nucleus-stained cells and their migration tracks in yellow. Scale bar = 100μm. (B) MSD(Δt) of WT cells fit with the Fürth model. (C) Cumulative distributions of the step length R for $\Delta t = 10$min. One blue curve per frame pair along a movie. The black line is a global fit of all blue curves with a cumulative Rayleigh distribution function. (D) Left: Schematic migration track and angular memory ($\cos\theta(\Delta t)$, see Materials and Methods) at $\Delta t = 10$min (yellow) and $\Delta t = 250$min (blue). Right: Angular memory ($\cos\theta(\Delta t)$) between $\Delta t = 10$min (yellow dot) and $\Delta t = 250$min (blue dot). Data of (B-D) from 94 cell tracks of 2 independent experiments. Mean $\pm$ SEM.

and both competed for by its head-tail interaction (Fig.2F).

Collectively migrating epithelial cells are superdiffusive, fractional Brownian walkers. To assess whether the same behavior and mechanisms apply to a cell collective, we tracked overnight nucleus-stained MDCK cells plated at confluence on collagen-coated glass coverslips (see Materials and Methods) (Fig. 3A, movie 3). In these conditions, the cell shape index (~ 4.2) was well above the rigidity threshold ($q \simeq 3.8$, Fig; S3A) (see Materials and Methods), which supports that the tissue behaved as a fluid with negligible resistance from cortical tension against cell rearrangements (48). We found that within the same time frame as in single cell migration experiments, cells no longer migrated as persistent random walkers, but adopted superdiffusive behavior with an anomalous exponent of about 1.7 (Fig. 3B, Table S2). Remarkably, this superdiffusive behavior allowed cells to eventually reach a greater distance than single cells in the same amount of time, even though their apparent speed was lower (Fig. S3B). To distinguish between the various walk models that could produce such a superdiffusive behavior (Lévy flight, fractional Brownian motion, or their combinations (7, 49)), we examined the step size distributions and found that they were consistent with a Gaussian walk on any time scale up to $\Delta t = 3$hrs (Fig. 3C, S3C). However, we found that the angular deviation of any 10min-step from the direction of the previous step was skewed toward small angles and invariant with the time scale of the previous step up to $\Delta t = 250$min (Fig. S3D). In other words, the angular memory never disappeared within our experimental time frame, unlike that of single cells (Fig. 3D compared to Fig. 1D). Gaussianity and virtually infinite directional memory are characteristics of a pure fractional Brownian motion and thus rule out Lévy walks or other combination. Cell superdiffusion thus emerges from a fractional Brownian motion.

The transition in directional memory emerges from Adherens Junction-mediated intercellular adhesion. To assess whether the transition from finite to infinite directional memory observed at confluence resulted from simple steric hindrance due to crowding by neighbor cells or from genuine AJ-mediated intercellular adhesion, we examined the collective migration of cells depleted of α-catenin, without which cells cannot form AJs (50)(see Materials and Methods). Remarkably, the cells lost most of their superdiffusive behavior (with an anomalous exponent α dropping to about 1.2) despite being as crowded as WT cells (Fig. 3E). Consistently, angular memory vanished in the experimental time frame (Fig. 3F), as for single migrating cells. Next, to test whether cadherin subtypes could compensate

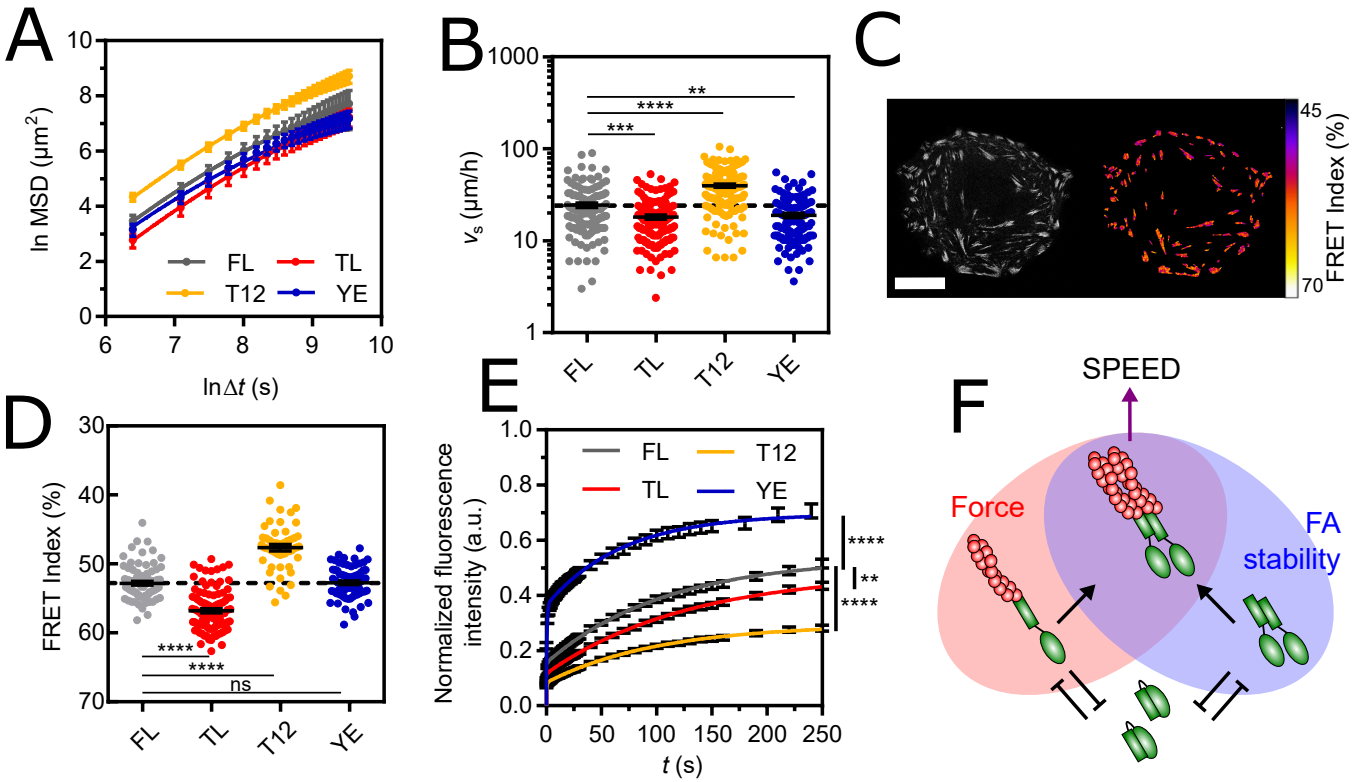

Fig. 2. (A) MSD(Δt) of vinculin FL and mutant cells fit with the Fürth model. (B) Apparent speed of single, vinculin FL and mutant cells. (C) Left: direct fluorescence of vinculin TSMod in a single cell. Right: FRET Index map (see Materials and Methods). Scale bar = 20 μm. (D) FRET Index of TSMod in the FL, TL, T12 and YE constructs in FAs. (E) Fluorescence recovery after photobleaching of FL, TL, T12 and YE constructs in FAs fit with a 2-phases association model. (F) Proposed model: at FAs, the head-tail interaction of vinculin (green) competes with both tail dimerization and actin filaments (red) binding, which provide FA stability and force transmission, respectively, together promoting cell speed. Data of (A,B) from 125 (FL), 129 (TL), 193 (T12) and 110 (YE) cell tracks of 3 independent experiments. Data of (D) from 81 (FL), 102 (TL), 52 (T12) and 84 (YE) cells of 4 (FL) and 3 (TL, T12, YE) independent experiments. Data of (E) from 105 (FL), 112 (TL), 118 (T12) and 65 (YE) cells of 2 independent experiments. Mean $\pm$ SEM. Two-tailed Mann-Whitney tests between each mutant and FL (B,D). Extra-sum-of-squares F test with shared immobile fraction between each mutant and FL as the null hypothesis (E).

for each other, we used cells depleted of E-cadherin but that retained cadherin-6 expression (50)(see Materials and Methods). These cells exhibited a slightly higher anomalous exponent than WT cells (Fig. 3E) and, consistently, infinite angular memory (Fig. 3F). This shows that E-cadherin specifically is largely dispensable, if not slightly detrimental, for cells to migrate in a superdiffusive manner, just as it is for the maintenance of AJs (50). Similarly, different cadherin subtypes can compensate for the defficiency of E-cadherin in other contexts (51–53).

The confluence-induced transition in directional memory is therefore the result of *bona fide* AJ-mediated intercellular adhesion, but independently of the cadherin subtype.

Velocity coordination between neighbors suffices to produce superdiffusion. Because velocity coordination is lost upon disruption of AJs by α-catenin depletion (Fig. S3E) (11), we sought to determine whether this effect of intercellular adhesion sufficed to confer a superdiffusive behavior to confluent cells regardless of other intercelullar adhesion features. To do so, we turned to *in silico* simulations of interacting self-propelled particles (SPP, see Materials and Methods). First, we modeled individual cells as persistent random walkers with the same apparent speed and intrinsic persistence P_0 in isolation for all cells, in compliance with single cell migration results. Accordingly, P_0 is directly proportional to the time τ needed to make a step and a function of the intrinsic directional freedom of the cell between each step. Then, we modeled velocity coordination with a classic Vicsek interaction within a cell-scale distance d (54), and explored the MSD of particles at densities ρ covering isolated cells up to beyond confluence. We found that as the number of interacting neighbors $n = \pi\rho d^2$ increased, the effective persistence P of the particles increasingly diverged from P_0 before the migration behavior transitioned to superdiffusion (Fig. 3G). Strikingly, for a range of realistic values of interaction distance $d \sim 10 - 30\mu$m, confluent density $\rho \sim 2000 - 4000$ cells/mm^2 and various degrees of directional freedom affecting $1 \lessapprox P_0/\tau \lessapprox 10$, the anomalous exponent fell around $\alpha \sim 1.7$ (yellow region), consistent with experimental observations (see Fig. 3).

Furthermore, this model predicted that provided a minimal number of interacting neighbors was reached, persistent random walkers would always transition to superdiffusers regardless of their intrinsic persistence. To test this, we tracked the single and collective cell migration of RPE-1 cells, another epithelial cell line (Fig. S3F, movies 4, 5). We found that single RPE-1 cell migration was also much better described by a persistent random walk than by a diffusion model, although with a persistence around 1 hr, making the difference hard to notice by eye within the experimental time

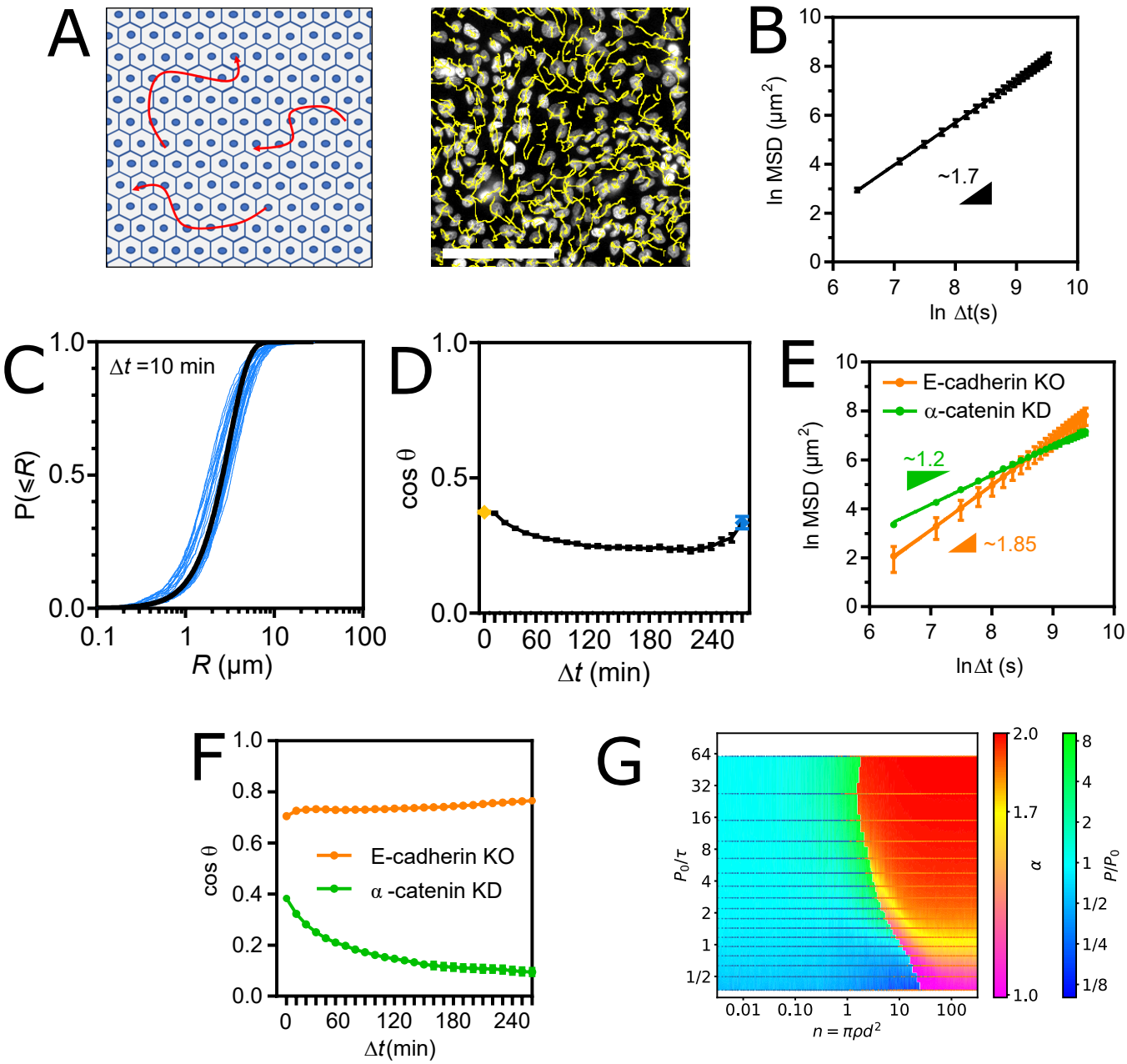

Fig. 3. (A) Left: Schematic representation of the collective cell migration assay. Right: fluorescence image of nucleus-stained cells and their migration tracks in yellow. Scale bar = 100μm. (B) MSD(Δt) of WT cells fit with a straight line in ln-ln scale . (C) Cumulative distributions of the step length R for $\Delta t = 10$min. One blue curve per frame pair along a movie. The black line is a global fit of all blue curves with a cumulative Rayleigh distribution function. (D) Angular memory ($\cos\theta(\Delta t)$) between $\Delta t = 10$min (yellow dot) and $\Delta t = 250$min (blue dot). (E) MSD(Δt) of E-cadherin KO and α-catenin KD cells fit with a straight line in ln-ln scale. (F) Angular memory ($\cos\theta(\Delta t)$) of E-cadherin KO and α-catenin KD cells. Data of (B-D) from 11 Fields Of View (FOV, 500-1000 tracks each) of 3 independent experiments. Data of (E-F) from 3 (E-cadherin KO) and 4 (α-catenin KD) FOV (500-100 tracks each) of 2 (E-cadherin KO) and 3 (α-catenin KD) independent experiments. Mean $\pm$ SEM. (G) Migration behavior of Self-Propelled Particles with Vicsek interactions as a function of P_0/τ and number of interacting neighbors $n = \pi\rho d^2$. Blue and orange points are simulation coordinates that resulted in persistent and super-diffusive behavior, respectively. Cold and warm color backgrounds are interpolations from points above of P/P_0 and α values, respectively.

window (Fig. S3E). Moreover, RPE-1 cell migration at confluence was again much better described by a superdiffusion model with an anomalous exponent around 1.6, as expected (Fig. S3E).

We conclude that velocity coordination is a feature of intercellular adhesion that suffices to produce superdiffusion at confluence in a manner that is very robust to the intrinsic persistence of cells, as predicted by our model.

Stabilization of Adherens Junctions by vinculin dimerization lowers cell migration speed. To further investigate the regulation of collective migration by intercellular adhesions, we examined the effects of confluence on vinculin mutant cell lines. All cell lines behaved as fluid tissues at confluence and their cells remained superdiffusive regardless of the expressed mutant (Fig. S4A, Fig. 4A, Table S3), showing that vinculin plays little to no role in the regulation of directional memory by intercellular adhesions. However, confluence affected cell migration speed differently depend-

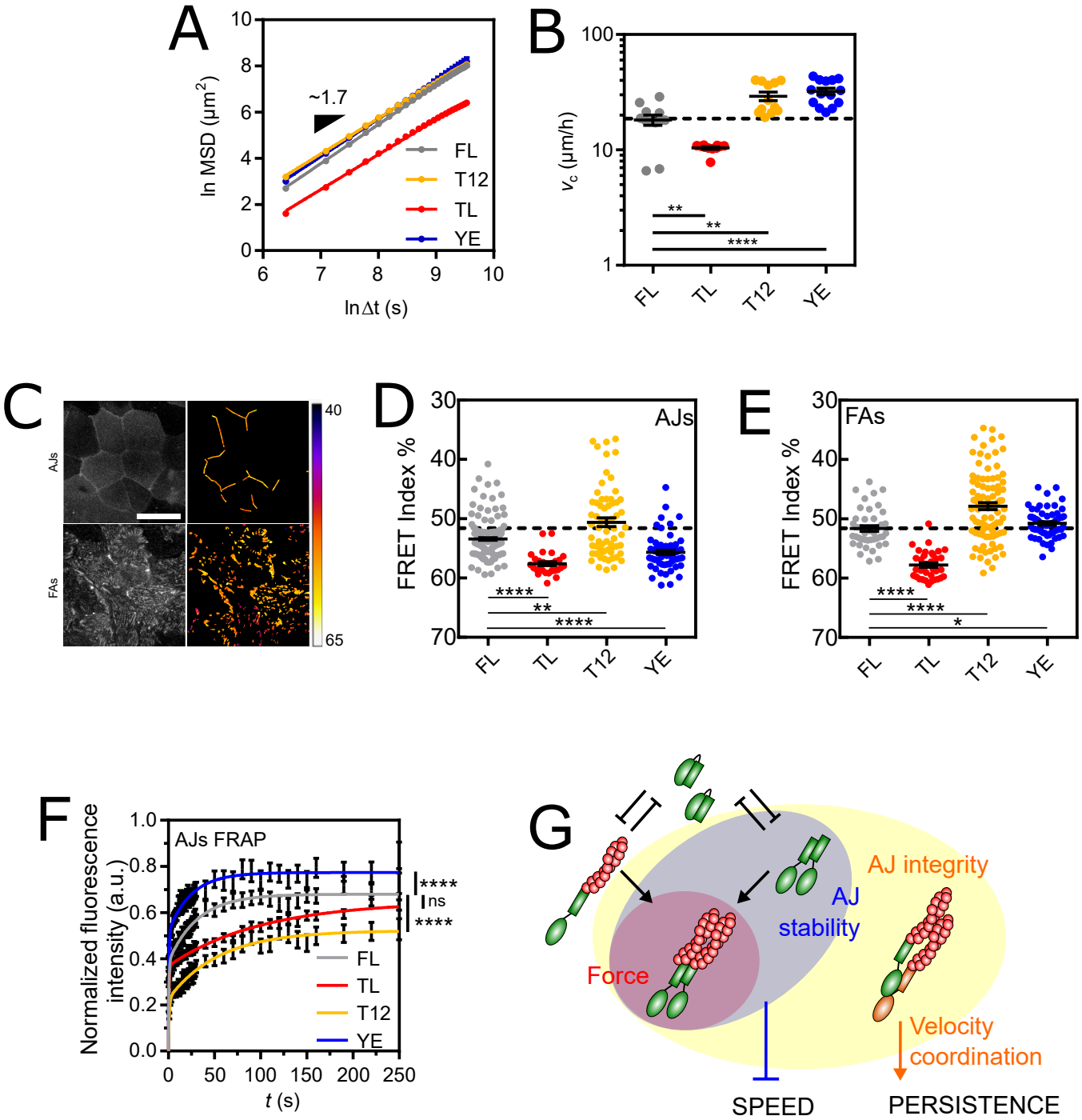

Fig. 4. (A) MSD(Δt) of vinculin FL and mutant cells fit with a straight line in ln-ln scale. (B) Apparent speed of vinculin FL and mutant cells at confluence. (C) Left: direct fluorescence of vinculin TSMod in a confluent monolayer. Right: FRET Index map (see Materials and Methods). Top: in the AJs plane. Bottom: in the FAs plane. Scale bar = 20μm. (D) FRET Index of TSMod in the FL, TL, T12 and YE constructs in AJs at confluence. (E) FRET Index of TSMod in the FL, TL, T12 and YE constructs in FAs at confluence. (F) Fluorescence recovery after photobleaching of FL, TL, T12 and YE constructs in AJs fit with a 2-phases association model. (G) Proposed model: at AJs, α-catenin (orange) provides AJ integrity (connection to the cytoskeleton), which promotes persistence. The head-tail interaction of vinculin (green) competes with both tail dimerization and actin filaments (red) binding. Dimerization provides AJ stability, which slows cell down. Data of (A-B) from 12 (FL), 11 (TL, T12) and 14 (YE) FOV (500-1000 tracks each) of 3 independent experiments. Data of (D) from 169 (FL), 30 (TL) and 64 (T12, YE) contacts of 5 (FL) and 3 (TL, T12, YE) independent experiments, and (E) from 45 (FL), 35 (TL), 104 (T12) and 67 (YE) cells of 4 (FL) and 3 (TL, T12, YE) independent experiments. Data of (F) from 75 (FL), 137 (TL), 78 (T12) and 36 (YE) contacts of 4 (FL, TL, T12) and 3 (YE) independent experiments. Mean $\pm$ SEM. Two-tailed Mann-Whitney tests between each mutant and FL (B,D,E). Extra-sum-of-squares F test with shared immobile fraction between each mutant and FL as the null hypothesis (F).

ing on the mutant, independently of cell density (Fig. S4B). Specifically, the TL and T12 mutants were slower and faster, respectively, compared to FL vinculin (Fig. 4B), just as they were when migrating in isolation (see Fig. 2B). By contrast, the YE mutant was faster than FL at confluence (Fig. 4B), while it was slightly slower in isolation (see Fig. 2B). Overall, confluence decreased cell migration speed in a manner that could be predicted from single cell speed for all but the YE mutant, which displayed faster cell migration at confluence than when isolated (Fig. S4C).

Mechanical tension in AJs promotes vinculin recruitment and tension (55). Thus, to investigate the mechanisms underlying this emergent regulation of migration speed, we examined the tension of vinculin at AJs (Fig. 4C). We found that vinculin experienced slightly less tension in AJs compared to FAs at confluence (Fig. 4D,E). Furthermore, the effects of the mutants on tension at confluence could be predicted from their effects in single cells for the TL and T12 mutants, which decreased and increased tension, respectively, but not for the YE mutant, which had a stronger effect at confluence than in single cells and opposite effects between FAs and AJs at confluence: while it increased tension in FAs, it decreased tension in AJs (Fig. S4D). Moreover, the YE mutant was responsible for the loss of correlation between vinculin tension and cell migration speed that now appeared at confluence (Fig. S4E).

The stability of AJs components is based on vinculin (18). Thus, to better understand how vinculin might combine its effects in FAs and AJs to regulate cell speed in such an emergent manner, we examined the stability of vinculin and its mutants in AJs by FRAP (Fig. S4F, movie 6). FRAP experiments showed that the YE mutant had a significantly smaller immobile fraction than FL vinculin, while the TL and T12 mutants had larger immobile fractions, just as in FAs, although only that of the T12 mutant was significantly different (Fig. 4F). In agreement, the two stable mutants also showed ectopic recruitment that extended along the lateral cell surface below the restricted apical location of FL (Fig. S4G).

Overall, these results support that when AJs are stable (TL, FL, T12), regardless of the tension they transmit via vinculin, cells collectively migrate more slowly but in proportion to their single cell migration speed. In contrast, when AJs are unstable (YE), cells collectively migrate proportionally faster than single cells. Therefore, we therefore propose that vinculin dimerization ensures the stability of AJs, which, independently of vinculin tension, adapts the collective cell migration speed to the single cell migration speed in an emergent manner (Fig. 4G).

Superdiffusion overcomes the weak directional bias caused by adhesion-dependent sensitivity to external guidance cues. Here, we sought to evaluate how the addition of an external guidance cue would affect the spatial exploration efficiency of collectively migrating cells. To do this, we wounded a confluent epithelial monolayer and tracked nucleus-stained cells as they invaded the free surface to close the wound (Fig. 5A, movie 7). Approximately 3 hours after wounding, the apparent speed of cells stabilized (Fig. S5A), consistent with previous reports (56), and was independent of the distance to the wound (Fig. S5B). Thus, we examined the MSD from 3hrs post-wound on. In principle, a directional bias eventually results in ballistic motion as Δt increases, so we expected the slope of the MSD to eventually tend toward 2 in ln-ln scale for large Δt. However, we found that migration behavior remained superdiffusive with an anomalous exponent around 1.6 (Fig. 5B). Furthermore, as in the case of unbiased collective migration, the anomalous exponent decreased to around 1.2 for cells depleted of α-catenin, whereas cells depleted of E-cadherin remained superdiffusive, (Fig. 5C). Similarly, vinculin mutants did not affect the superdiffusive behavior (Fig. 5D). Overall, these results show that the mechanisms that govern the persistence of collective cell migration do not differ substantially in the presence or absence of an external guidance cue on the scale of a few hours.

We therefore sought to assess the time scale at which the guidance cue would significantly bias cell migration velocity, as well as the magnitude of this bias. In the steady state speed regime (at 6hrs), a directional bias was already visible at the 10 min scale, i.e. on the apparent cell velocity (Fig. 5E). The bias appeared within 3hrs post-wound and remained stable throughout (Fig. 5F). This shows that a directional bias of such magnitude at $\Delta t = 10$min that is maintained from 3hrs onwards is too weak to substantially improve the spatial reach of collectively migrating cells in the time range of the experiment. Finally, we asked whether disrupted AJs would alter the sensitivity of cells to directional bias in addition to migration persistence. Remarkably, cells depleted of α-catenin exhibited very little directional bias compared to WT cells (Fig. 5F). Together, this shows that AJ-mediated intercellular adhesion is required not only for cells to acquire virtually infinite directional memory, but also for them to perceive external guidance cues.

Vinculin dimerization scales wound healing rate to the collective cell migration speed through the regulation of Adherens Junction mechanosensitivity. Because an external guidance cue did not affect the persistence of collective cell migration, we expected that the apparent speed of collectively migrating cells would predict the rate of wound healing, at which the wounded epithelium covers the free surface (see Materials and Methods). We found that this was mostly the case, with the exception of the YE mutant. Indeed, while vinculin FL, T12 and TL cells closed the wound at a rate proportional to their migration speed in the collective, YE mutant cells were less efficient in wound healing than expected (Fig. 6A). This supports that vinculin dimerization, in contrast to other vinculin tail interactions, affects collective migration speed in a manner dependent of external guidance cues, in addition to its role in scaling collective cell migration speed to single cell migration speed through AJs stability in an unbiased context (see Fig. 4). To determine how such an effect might emerge from this mutant, we evaluated how adhesions mechanically perceived biased collective cell migration (Fig. 6B-E). Indeed, we had previously found that biased collective migration of epithelial cells imprints

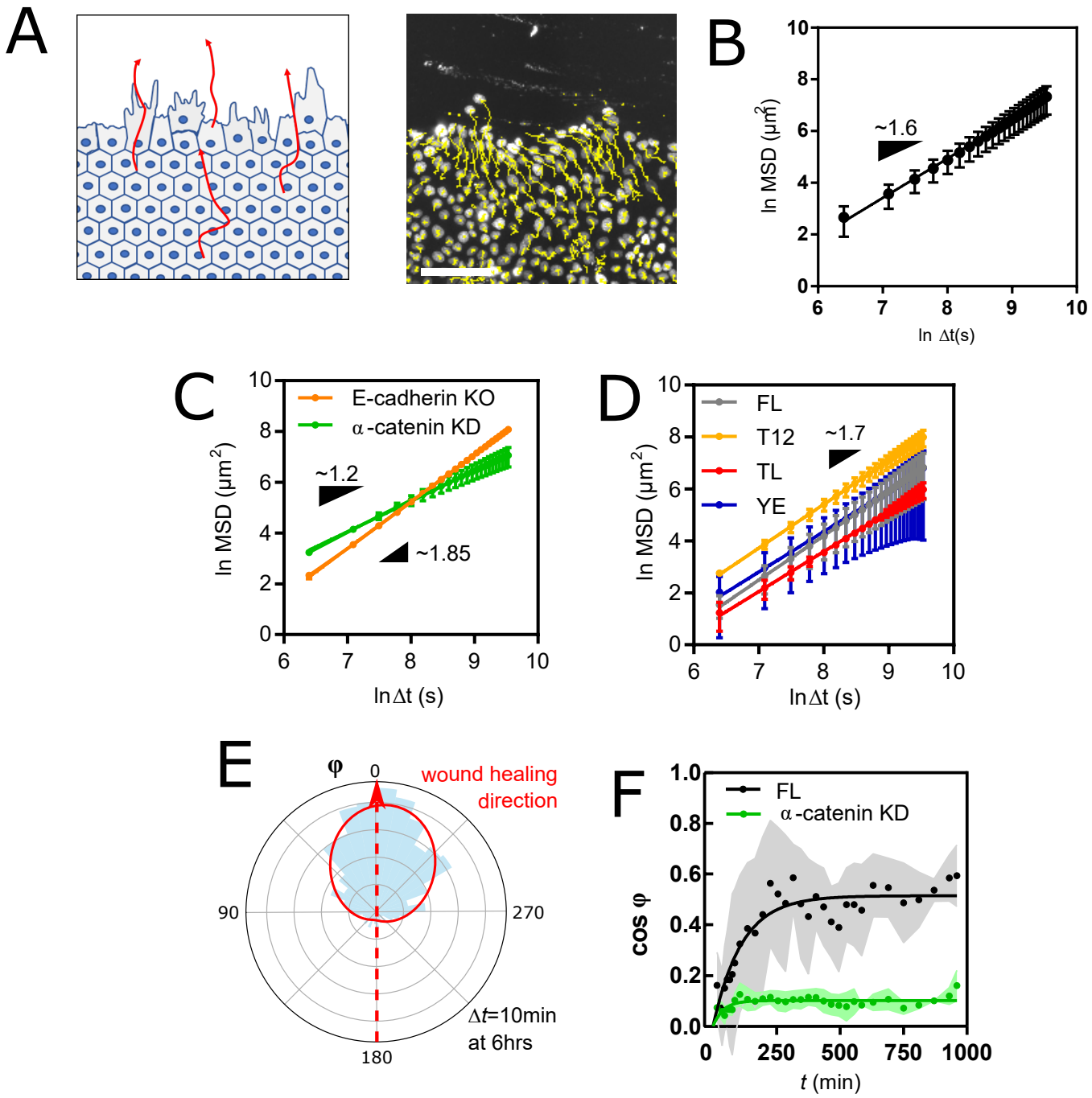

Fig. 5. (A) Left: Schematic representation of the guided collective cell migration assay. Right: fluorescence image of nucleus-stained cells and their migration tracks in yellow. Scale bar = 100μm. (B) MSD(Δt) of WT cells fit with a straight line in ln-ln scale. (C) MSD(Δt) of E-cadherin KO and α-catenin KD cells fit with a straight line in ln-ln scale. (D) MSD(Δt) of vinculin FL and mutant cells fit with a straight line in ln-ln scale. (E) Angular distribution of apparent velocities of vinculin FL cells at 6hrs post-wound fitted with a Von Mises distribution giving a concentration $\kappa \sim 1.3$ (solid red line). (F) Directionality ($\cos\phi(t)$, see Materials and Methods) of vinculin FL and α-catenin KD cells. All data from 4 (all but YE) and 3 (YE) FOV (500-1000 tracks each) of 4 (all but YE and α-catenin KD) and 3 (YE, α-catenin KD) independent experiments. Mean $\pm$ SEM.

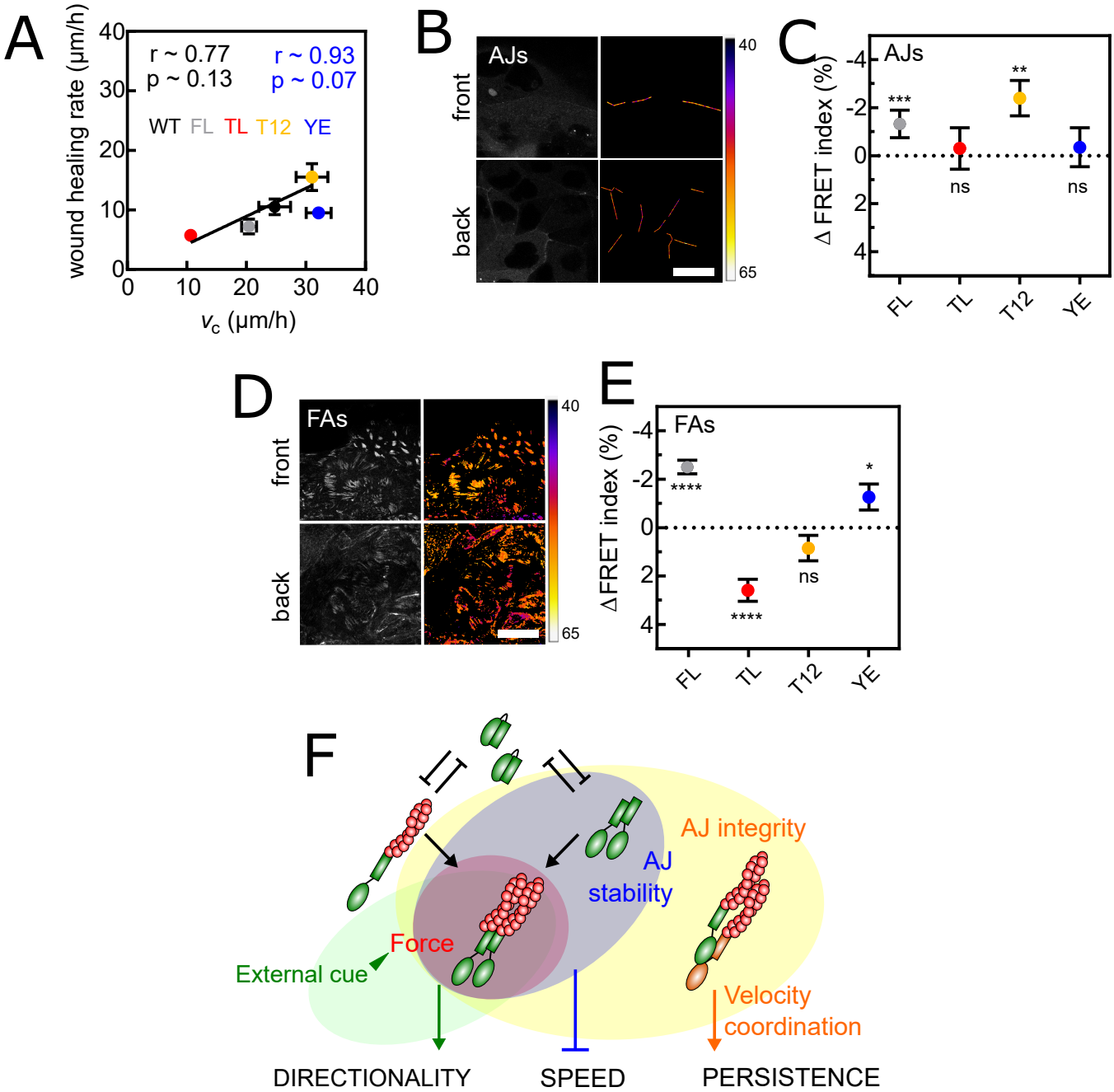

Fig. 6. (A) Wound healing rate (see Materials and Methods) as a function of cell speed at confluence for WT, vinculin FL and mutant cells. Pearson coefficients r and p-values in black for all data, in blue minus YE. (B) Left: direct fluorescence of vinculin TSMod in the AJs plane of cells at the wound front (top) and back (bottom). Right: corresponding FRET Index maps. (C) FRET Index difference between front and back cells at AJs of TSMod in vinculin FL and mutants. (D) Left: direct fluorescence of vinculin TSMod in the FAs plane of cells at the wound front (top) and back (bottom). Right: corresponding FRET Index maps. (E) FRET Index difference between front and back cells at FAs of TSMod in vinculin FL and mutants. (F) Proposed model: at AJs, vinculin dimerization and actin binding provide mechanosensitivity to stable AJs, which promotes wound healing. Data of (A) from 4 (all but YE) and 3 (YE) FOV of 4 (all but YE) and 3 (YE) independent experiments. Data of (C) from 55 (FL), 16 (TL), 56 (T12) and 26 (YE) front cells and 122 (FL), 30 (TL), 71 (T12) and 48 (YE) back cells of 4 (FL, T12) and 3 (TL, YE) independent experiments. Data of (E) from 144 (FL), 63 (TL), 124 (T12) and 46 (YE) front cells and 155 (FL), 84 (TL), 128 (T12) and 51 (YE) back cells of 7 (FL, T12), 4 (TL) and 3 (YE) independent experiments. Mean $\pm$ SEM. Two-tailed Mann-Whitney test between front and back cells for each construct (C,E). Scale bars = 50μm.

a transcellular gradient of molecular tension in E-cadherins, which are under higher tension away from the migration front (57). Consistently, we found that FL vinculin was increasingly recruited and was under increased tension in AJs away from the migrating front, as was the T12 mutant (Fig. 6C). As expected, the TL mutant showed no mechanosensitivity and, remarkably, neither did the YE mutant (Fig. 6C). In FAs, the TL mutant, which is insensitive to cytoskeletal tension by design, displayed a differential in FRET suggesting a cytoskeleton-independent increase in vinculin compression from the migration front, as previously seen within single fibroblasts on adhesive patterns (58). In contrast, FL vinculin showed an opposite FRET differential, supporting that increased tension from front to back cells, as in AJs, overcompensates for cytoskeleton-independent compression specific to FAs. The T12 mutant showed no FRET gradient, suggesting that its increased cytoskeleton-independent compression from front to back cells is balanced by its increased cytoskeleton-dependent tension. Finally, the YE mutant exhibited a mechanosensitivity similar to that of FL vinculin (Fig. 3E). Together, this shows that the impaired mechanosensitivity of the YE mutant is specific to AJs and that the differential mechanosensitivity between FAs and AJs is specific to this mutant.

Overall, this supports that the wound healing rate scales with collective migration speed provided that the mechanosensitivity between AJs and FAs is balanced, a feature that depends on the dimerization of vinculin in AJs (Fig. 6F).

Discussion

In this work, we studied the exploratory capacity of epithelial cells, the influence of cell interactions and guidance cues on this exploration, and the dynamics and mechanics of the adhesion complexes that cells use in this process. Remarkably, we show that intercellular adhesion with neighbor cells within the epithelium provides virtually infinite directional memory for migration, as a result of velocity coordination. Mechanistically, our results support that cell speed depends on FAs stability and force transmission and is facilitated by AJs mobility, both controlled by vinculin. Finally, we show a specific role for vinculin dimerization in AJs, which regulates the mechanosensitivity of the epithelium as a whole to the guidance cue of a wound, and the wound healing rate of the epithelium.

Locomotion patterns of single cells have been observed and quantified for decades and can take many forms. When endowed with directional persistence arising from angular correlations between consecutive unit steps, cells adopt a so-called persistent random walk eventually converging toward a purely diffusive behavior, as initially observed in fibroblasts or single endothelial cells (4, 5). In contrast, in T cells and some metastatic cells that behave like Lévy walkers, the fat-tailed power-law distribution of step size is sufficient to support a super-diffusive behavior, even in the absence of temporal correlation in direction (7, 8). Here, our results are consistent with single cells undergoing a persistent random walk, with persistence on the order of several minutes to an hour depending on the cell line, beyond which cells purely diffuse (Fig. 1). Thus, the persistence of our epithelial cells is in the low range compared to individual endothelial cells, whose persistence time can reach several hours (5). Furthermore, comparing cell lines that express various forms of vinculin mutants, we observe that persistence does not correlate with cell speed, consistent with endothelial cells exposed to growth factors (5). Mechanistically, both cell speed and persistence are under the control of actin retrograde flow, via connections with cell-matrix adhesions for the former, and control of polarity factors for the latter (59). Our data are thus consistent with the idea that abnormal connection of cell-matrix adhesions to the cytoskeleton via vinculin uncouples speed from persistence.

Previously, vinculin-KO fibroblasts or epithelial cells have been shown to migrate faster than their WT counterparts (21, 22, 29). Here, we show that the migration speed of epithelial cells decreases with the expression of FL vinculin above endogenous levels (Fig. 1). Overall, this is consistent with the idea that the bulk effect of vinculin expression is a decrease in cell speed, as if vinculin were acting primarily as a migration moderator. Mechanistically, our results support that the head-tail interaction of vinculin challenges both vinculin force transmission and stability in FAs, as has been observed in other cell types (30, 39, 44–47), and is countered by the actin-vinculin tail interaction, which provides force transmission but is unnecessary for stability, and the dimerization of the tail, which promotes stability and is dispensable for force transmission (Fig. 2D,E). Overall, the combination of maximum force transmission and stability predicts maximum cell speed (Fig. 2B). Therefore, we propose that the speed of single cells is the product of force transmission and stability in FAs (Fig. 2F, S5C).

At confluence, we show that epithelial cells adopt a superdiffusive behavior that a persistent random walk cannot explain (Fig. 2). This behavior has previously been observed in single cells or in a collective for a variety of cell types (6–8, 13–15). However, whenever a model explained this behavior, it implied non-Gausian displacement distributions, which are sufficient to support superdiffusion without long-term memory. Moreover, it was not known whether superdiffusion in the collective originated from intercellular interactions or resulted from cells already walking alone in this manner. Here, we show that superdiffusion can be explained by a pure fractional Brownian motion, with Gaussian distribution of displacement, but with virtually infinite directional memory (Fig. 2A-D).

Previously, subdiffusive fractional Brownian motion has explained subcellular particle mobility in the crowded cytoplasm through interactions with the viscoelastic medium (60). Here in comparison, we show that a strong superdiffusive fractional Brownian motion emerges from intercellular adhesion mediated by cytoskeleton-bound but cadherin type-independent AJs, and not just steric hindrance due to the mere presence of neighboring cells (Fig. 3E,F). Remarkably, the same AJ-based mechanism also allows for velocity coordination between neighboring cells (Fig. S3E) (11).

While the interplay between persistent migration and elastic coupling provided by AJs was shown to be sufficient for velocity coordination (61), we further show here with our minimal agent-based model that such coordination is sufficient to explain the transition to superdiffusion under physiological conditions (Fig. 3G). In particular, the transition occurs for a number of interacting neighbors $n \sim 6$, about the number of direct neighbors at confluence. For MDCK cells with persistence $P_0 \sim 10$min, this would correspond to a step time τ of a few minutes. For RPE-1 cells with persistence $P_0 \sim 1$hr, τ would rather be several tens of minutes to an hour. This suggests that RPE-1 cells are more persistent due to their longer decision time, rather than narrower directional freedom. Notably, the decision time τ is intrinsic to persistent random walks but can be experimentally discriminated from directional freedom only upon interaction with neighbors. Discovering the respective molecular determinants of decision time and directional freedom appears as an exciting future research direction. In the same modeling context, others have shown that velocity coordination also results in spontaneous fluctuations in particle density (62). We thus propose that at confluence, such spatiotemporal fluctuations in the number of interacting neighbors generate variations in instantaneous persistence of cells along their trajectories, ultimately resulting in a distribution of persistence times across time scales. Consistently, the slope of the MSD(Δt) (in log scale) of a persistent random walk at time P is $e-1$, which is about the anomalous exponent α we observe, as if superdiffusing cells experienced a distribution of persistence times that spanned all our experimentally accessible time scales.

In addition to inducing a transition from finite to infinite directional memory, we show that intercellular adhesion globally decreases the apparent speed of cells, provided that vinculin is stable at AJs. Indeed, perturbation of vinculin dimerization leads to its low stability at AJs and faster than expected cell migration (Fig. 4B,F, S4C). Remarkably, this increase in cell speed is not the result of relaxed constraints on cortical deformations, as seen previously in unjamming transitions (63, 64), since vinculin mutants exhibit similar shapes indicative of a fluid phase (Fig. S4A). Alternatively, we speculate that the destabilization of AJs results in deeper intracellular changes within the cell's bulk, possibly due to the impaired ability to bundle actin of the vinculin mutant (41). This could therefore decrease the cell's own resistance to the bulk deformation required for migration but in a collective context only, and thus facilitate migration despite a less efficient FA machinery. Future studies may address this hypothesis.

Overall, intercellular adhesion normally impairs apparent cell speed but induces long-term directional persistence. As a result, while cells are collectively less efficient than single cells in exploring space at time scales of less than 3hrs, they can become more efficient beyond that (Fig. S3B). Thus, this emergence of long-term collective persistence may have a profound impact on tissue morphogenesis, regeneration, and homeostasis in a variety of contexts. In the case of wound healing, cells are further exposed to an external guidance cue. Here we show that this signal is sufficient to bias the velocity of each cell at the smallest experimental time scale (Fig. 5E). Detection of this signal is an emergent property of the collective, as disrupting intercellular adhesion renders cells nearly blind to free space (Fig. 5F). This is reminiscent of collective durotaxis and chemotaxis (65, 66). However, we show that this directional bias remains too small to drive ballistic motion in less than the longer experimental time range, such that cells remain superdiffusive throughout (Fig. 5A-D). Consistently, wound healing rates reach only a fraction of apparent cell speeds and in a manner that depends on vinculin tail dimerization (Fig. 6A). In this context, vinculin tail dimerization provides equal mechanosensitivity to AJs and FAs, so that they transmit molecular tension gradients across the tissue (Fig. 6B-E). This is again consistent with the requirements for supracellular durotaxis, which arises from intercellular force transmission (65), and may be related to the ability of cells to stiffen under force in a way that depends on vinculin dimerization (41). Finally, we expect the directional bias to lead to more ballistic cell motion at longer time scales, with a lower limit of at least 3hrs.

In summary, we conclude that the spatial exploration efficiency of guided collective migration depends on the scale considered: at short time scales (<3hrs for MDCK cells), the intrinsic migration speed of individual cells is the limit, which can be overcome by collective directional memory at intermediate time scales (>3hrs for MDCK cells), a tissue-level property that guidance cues from the environment must override to become significant at longer time scales (»3hrs) (Fig. S5D). We speculate that this generic framework applies qualitatively to guided collective migration in general and hope that future studies will test this prediction.

Materials and Methods

Live MDCK type II G cells stably expressing fluorescently tagged proteins were monitored on a wide-field epifluorescence inverted microscope for migration experiments, on a scanning spectral confocal microscope for FRET experiments, or on a spinning disk confocal microscope for FRAP experiments. Image analyses were performed with Imaris and ImageJ, data analyses with Matlab and statistics with Prism software. Full materials and methods are available in Supplementary Materials and Methods.

ACKNOWLEDGEMENTS

We thank the members of the laboratory, C. Leclainche, S. Etienne-Manneville, B. Ladoux, P. Ronceray and R. Voituriez for insightful discussions. We thank C. Grashoff (Westfälische Wilhelms-Universität Münster), B. Ladoux and R.-M. Mège (Institut Jacques Monod), W. James Nelson (Stanford U.) and K. Schauer (Institut Gustave Roussy) for the gift of plasmids and cell lines. This work was supported in part by the Centre national de la recherche scientifique (CNRS), the French National Research Agency (ANR) grants (ANR-17-CE13-0013, ANR-17-CE09-0019, ANR-18-CE13-0008, ANR-21-CE13-0048), the Investments for the Future program of the French Government (LabEx Who am I? ANR-11-LABX-0071, Université Paris Cité ANR-18-IDEX-0001) and the Association pour la Recherche contre le Cancer (ARC-PJA22020060002255). We acknowledge the ImagoSeine facility, member of the France BioImaging infrastructure (ANR-10-INSB-04), and the Institut Jacques Monod IT team. HC was supported by La Ligue contre le Cancer (TAYS18872) and Fondation Recherche Médicale (FDT202001010843).

References

1. Peter Friedl and Darren Gilmour. Collective cell migration in morphogenesis, regeneration and cancer. *Nature Reviews Molecular Cell Biology 2009 10:7*, 10(7):445–457, jul 2009.

ISSN 1471-0080. doi: 10.1038/NRM2720.
2. Peter Friedl and Katarina Wolf. Plasticity of cell migration: a multiscale tuning model. *The Journal of cell biology*, 188(1):11–19, 2010. doi: 10.1083/jcb.200909003.
3. M Abercrombie and Joan E M Heaysman. Observations on the social behaviour of cells in tissue culture : I. Speed of movement of chick heart fibroblasts in relation to their mutual contacts. *Experimental Cell Research*, 5(1):111–131, 1953.
4. Mitchell H. Gail and Charles W. Boone. The Locomotion of Mouse Fibroblasts in Tissue Culture. *Biophysical Journal*, 10(10):980–993, oct 1970. ISSN 00063495. doi: 10.1016/S0006-3495(70)86347-0.
5. C.L. Stokes, D.A. Lauffenburger, and S.K. Williams. Migration of individual microvessel endothelial cells: stochastic model and parameter measurement. *Journal of Cell Science*, 99(2), 1991.
6. Peter Dieterich, Rainer Klages, Roland Preuss, and Albrecht Schwab. Anomalous dynamics of cell migration. *Proceedings of the National Academy of Sciences of the United States of America*, 105(2):459–463, jan 2008. ISSN 00278424. doi: 10.1073/pnas.0707603105.
7. Tajie H. Harris, Edward J. Banigan, David A. Christian, Christoph Konradt, Elia D.Tait Wojno, Kazumi Norose, Emma H. Wilson, Beena John, Wolfgang Weninger, Andrew D. Luster, Andrea J. Liu, and Christopher A. Hunter. Generalized Lévy walks and the role of chemokines in migration of effector CD8 + T cells. *Nature*, 486(7404):545–548, jun 2012. ISSN 00280836. doi: 10.1038/nature11098.
8. Sabil Huda, Bettina Weigelin, Katarina Wolf, Konstantin V. Tretiakov, Konstantin Polev, Gary Wilk, Masatomo Iwasa, Fateme S. Emami, Jakub W. Narojczyk, Michal Banaszak, Siowling Soh, Didzis Pilans, Amir Vahid, Monika Makurath, Peter Friedl, Gary G. Borisy, Kristiana Kandere-Grzybowska, and Bartosz A. Grzybowski. Lévy-like movement patterns of metastatic cancer cells revealed in microfabricated systems and implicated in vivo. *Nature Communications*, 9(1):1–11, dec 2018. ISSN 20411723. doi: 10.1038/s41467-018-06563-w.
9. B. Szabó, G. J. Szöllösi, B. Gönci, Zs Jurányi, D. Selmeczi, and Tamás Vicsek. Phase transition in the collective migration of tissue cells: Experiment and model. *Physical Review E - Statistical, Nonlinear, and Soft Matter Physics*, 74(6):061908, dec 2006. ISSN 15393755. doi: 10.1103/PHYSREVE.74.061908/FIGURES/5/MEDIUM.
10. Philip Vitorino, Mark Hammer, Jongmin Kim, and Tobias Meyer. A Steering Model of Endothelial Sheet Migration Recapitulates Monolayer Integrity and Directed Collective Migration. *Molecular and Cellular Biology*, 31(2):342–350, jan 2011. doi: 10.1128/MCB.00800-10.
11. N. Borghi, M. Lowndes, V. Maruthamuthu, M.L. Gardel, and W.J. Nelson. Regulation of cell motile behavior by crosstalk between cadherin- and integrin-mediated adhesions. *Proceedings of the National Academy of Sciences of the United States of America*, 107(30), 2010. ISSN 10916490. doi: 10.1073/pnas.1002662107.
12. Adam Shellard and Roberto Mayor. Rules of collective migration: From the wildebeest to the neural crest: Rules of neural crest migration. *Philosophical Transactions of the Royal Society B: Biological Sciences*, 375(1807), sep 2020. ISSN 14712970. doi: 10.1098/rstb.2019.0387.
13. Hisashi Haga, Chikako Irahara, Ryo Kobayashi, Toshiyuki Nakagaki, and Kazushige Kawabata. Collective Movement of Epithelial Cells on a Collagen Gel Substrate. *Biophysical Journal*, 88(3):2250–2256, mar 2005.
14. Kenechukwu David Nnetu, Melanie Knorr, Steve Pawlizak, Thomas Fuhs, and Josef A. Käs. Slow and anomalous dynamics of an MCF-10A epithelial cell monolayer. *Soft Matter*, 9(39): 9335–9341, sep 2013. ISSN 1744-6848. doi: 10.1039/C3SM50806D.
15. Tatiane Souza Vilela Podestá, Tiago Venzel Rosembach, Anésia Aparecida Dos Santos, and Marcelo Lobato Martins. Anomalous diffusion and q-Weibull velocity distributions in epithelial cell migration. *PLoS ONE*, 12(7), jul 2017. ISSN 19326203. doi: 10.1371/journal.pone.0180777.
16. Michael P. Sheetz, Dan P. Felsenfeld, and Catherine G. Galbraith. Cell migration: regulation of force on extracellular-matrix-integrin complexes. *Trends in cell biology*, 8(2):51–54, 1998. ISSN 0962-8924. doi: 10.1016/S0962-8924(98)80005-6.
17. Nathalie Q Balaban, Ulrich S Schwarz, Daniel Riveline, Polina Goichberg, Gila Tzur, Ilana Sabanay, Diana Mahalu, Sam Safran, Alexander Bershadsky, Lia Addadi, and Benjamin Geiger. Force and focal adhesion assembly: a close relationship studied using elastic micropatterned substrates. *Nat Cell Biol*, 3(5):466–472, may 2001. ISSN 1465-7392.
18. Shigenobu Yonemura, Yuko Wada, Toshiyuki Watanabe, Akira Nagafuchi, and Mai Shibata. Alpha-Catenin as a tension transducer that induces adherens junction development. *Nature cell biology*, 12(6):533–542, 2010. ISSN 1465-7392. doi: 10.1038/ncb2055.
19. Robert P. Johnson and Susan W. Craig. Actin Activates a Cryptic Dimerization Potential of the Vinculin Tail Domain. *Journal of Biological Chemistry*, 275(1):95–105, jan 2000. ISSN 0021-9258. doi: 10.1074/JBC.275.1.95.
20. Mitsuko Watabe-Uchida, Naoshige Uchida, Yuzo Imamura, Akira Nagafuchi, Kazushi Fujimoto, Tadashi Uemura, Stefan Vermeulen, Frans van Roy, Eileen D Adamson, and Masatoshi Takeichi. alpha -Catenin-Vinculin Interaction Functions to Organize the Apical Junctional Complex in Epithelial Cells. *The Journal of Cell Biology*, 142(3):847–857, aug 1998.
21. Karry M Jannie, Shawn M Ellerbroek, Dennis W Zhou, Sophia Chen, David J Crompton, Andrés J García, and Kris A DeMali. Vinculin-dependent actin bundling regulates cell migration and traction forces. *The Biochemical journal*, 465(3):383–93, feb 2015. ISSN 1470-8728. doi: 10.1042/BJ20140872.
22. Hyunna T. Lee, Lisa Sharek, E. Timothy O'Brien, Fabio L. Urbina, Stephanie L. Gupton, Richard Superfine, Keith Burridge, and Sharon L. Campbell. Vinculin and metavinculin exhibit distinct effects on focal adhesion properties, cell migration, and mechanotransduction. *PLOS ONE*, 14(9):e0221962, sep 2019. ISSN 1932-6203. doi: 10.1371/journal.pone.0221962.
23. M Cecilia Subauste, Olivier Pertz, Eileen D Adamson, Christopher E Turner, Sachiko Junger, and Klaus M Hahn. Vinculin modulation of paxillin-FAK interactions regulates ERK to control survival and motility. *The Journal of cell biology*, 165(3):371–81, may 2004. ISSN 0021-9525. doi: 10.1083/jcb.200308011.
24. W Xu, JL Coll, and ED Adamson. Rescue of the mutant phenotype by reexpression of full-length vinculin in null F9 cells; effects on cell locomotion by domain deleted vinculin. *J. Cell Sci.*, 111(11):1535–1544, jun 1998.
25. Aniqua Rahman, Shawn P. Carey, Casey M. Kraning-Rush, Zachary E. Goldblatt, Francois Bordeleau, Marsha C. Lampi, Deanna Y. Lin, Andrés J. García, and Cynthia A. Reinhart-King. Vinculin regulates directionality and cell polarity in two-And three-dimensional matrix and three-dimensional microtrack migration. *Molecular Biology of the Cell*, 27(9):1431–1441, may 2016. ISSN 19394586. doi: 10.1091/MBC.E15-06-0432/ASSET/IMAGES/LARGE/MBC-27-1431-G007.JPEG.
26. J. R. Carvalho, I. C. Fortunato, C. G. Fonseca, A. Pezzarossa, P. Barbacena, M. A. Dominguez-Cejudo, F. F. Vasconcelos, N. C. Santos, F. A. Carvalho, and Claudio A. Franco. Non-canonical Wnt signaling regulates junctional mechanocoupling during angiogenic collective cell migration. *eLife*, 8, jun 2019. ISSN 2050084X. doi: 10.7554/eLife.45853.001.
27. Jianzhong Ai, Tao Jin, Lu Yang, Qiang Wei, Yang Yang, Hong Li, Ye Zhu, Jianzhong Ai, Tao Jin, Lu Yang, Qiang Wei, Yang Yang, Hong Li, and Ye Zhu. Vinculin and filamin-C are two potential prognostic biomarkers and therapeutic targets for prostate cancer cell migration. *Oncotarget*, 8(47):82430–82436, jul 2017. ISSN 1949-2553. doi: 10.18632/ONCOTARGET.19397.
28. Stefan Moese, Matthias Selbach, Volker Brinkmann, Alexander Karlas, Beatrice Haimovich, Steffen Backert, and Thomas F. Meyer. The Helicobacter pylori CagA protein disrupts matrix adhesion of gastric epithelial cells by dephosphorylation of vinculin. *Cellular Microbiology*, 9(5):1148–1161, may 2007. ISSN 1462-5822. doi: 10.1111/J.1462-5822.2006.00856.X.
29. J. L. Coll, A. Ben-Ze'ev, R. M. Ezzell, J. L. Rodríguez Fernández, H. Baribault, R. G. Oshima, and E. D. Adamson. Targeted disruption of vinculin genes in F9 and embryonic stem cells changes cell morphology, adhesion, and locomotion. *Proceedings of the National Academy of Sciences of the United States of America*, 92(20):9161–9165, sep 1995. ISSN 00278424. doi: 10.1073/pnas.92.20.9161.
30. Alex Carisey, Ricky Tsang, Alexandra M Greiner, Nadja Nijenhuis, Nikki Heath, Alicja Nazgiewicz, Ralf Kemkemer, Brian Derby, Joachim Spatz, and Christoph Ballestrem. Vinculin regulates the recruitment and release of core focal adhesion proteins in a force-dependent manner. *Current Biology*, 23(4):271–81, feb 2013. ISSN 1879-0445. doi: 10.1016/j.cub.2013.01.009.
31. Jennifer L Bays, Xiao Peng, Catlin E Tolbert, Christophe Guilluy, Ashley E Angell, Yuan Pan, Richard Superfine, Keith Burridge, and Kris A DeMali. Vinculin phosphorylation differentially regulates mechanotransduction at cell-cell and cell-matrix adhesions. *The Journal of cell biology*, 205(2):251–63, apr 2014. ISSN 1540-8140. doi: 10.1083/jcb.201309092.
32. Katheryn E. Rothenberg, David W. Scott, Nicolas Christoforou, and Brenton D. Hoffman. Vinculin Force-Sensitive Dynamics at Focal Adhesions Enable Effective Directed Cell Migration. *Biophysical Journal*, 114(7):1680–1694, apr 2018. ISSN 0006-3495. doi: 10.1016/J.BPJ.2018.02.019.
33. Jacqueline M Benjamin, Adam V Kwiatkowski, Changsong Yang, Farida Korobova, Sabine Pokutta, Tatyana Svitkina, William I Weis, and W James Nelson. Alpha-E-catenin regulates actin dynamics independently of cadherin-mediated cell–cell adhesion. *Journal Of Cell Biology*, 189(2):339–352, 2010. doi: 10.1083/jcb.200910041.
34. Rima Seddiki, Gautham Hari Narayana Sankara Narayana, Pierre-Olivier Strale, Hayri Emrah Balcioglu, Grégoire Peyret, Mingxi Yao, Anh Phuong Le, Chwee Teck Lim, Jie Yan, Benoit Ladoux, and René Marc Mège. Force-dependent binding of vinculin to α-catenin regulates cell-cell contact stability and collective cell behavior. *Molecular biology of the cell*, 29(4):380–388, feb 2018. ISSN 1939-4586. doi: 10.1091/mbc.E17-04-0231.
35. Reinholdrth Fürth. Die Brownsche Bewegung bei Berücksichtigung einer Persistenz der Bewegungsrichtung. Mit Anwendungen auf die Bewegung lebender Infusorien. *Zeitschrift für Physik*, 2(3):244–256, jun 1920. ISSN 14346001. doi: 10.1007/BF01328731.
36. G. E. Uhlenbeck and L. S. Ornstein. On the theory of the Brownian motion. *Physical Review*, 36(5):823–841, sep 1930. ISSN 0031899X. doi: 10.1103/PhysRev.36.823.
37. Carsten Grashoff, B.D. Hoffman, M.D. Brenner, Ruobo Zhou, Maddy Parsons, M.T. Yang, M.A. McLean, S.G. Sligar, C.S. Chen, Taekjip Ha, and Others. Measuring mechanical tension across vinculin reveals regulation of focal adhesion dynamics. *Nature*, 466(7303): 263–266, 2010. doi: 10.1038/nature09198.
38. Matthew G Rubashkin, Luke Cassereau, Russell Bainer, Christopher C DuFort, Yoshihiro Yui, Guanqing Ou, Matthew J Paszek, Michael W Davidson, Yunn-Yi Chen, and Valerie M Weaver. Force engages vinculin and promotes tumor progression by enhancing PI3K activation of phosphatidylinositol (3,4,5)-triphosphate. *Cancer research*, 74(17):4597–611, sep 2014. ISSN 1538-7445. doi: 10.1158/0008-5472.CAN-13-3698.
39. Jonathan D Humphries, Pengbo Wang, Charles Streuli, Benny Geiger, Martin J Humphries, and Christoph Ballestrem. Vinculin controls focal adhesion formation by direct interactions with talin and actin. *The Journal of Cell Biology*, 179(5):1043–1057, dec 2007.
40. Daniel M Cohen, Hui Chen, Robert P Johnson, Begum Choudhury, and Susan W Craig. Two distinct head-tail interfaces cooperate to suppress activation of vinculin by talin. *The Journal of biological chemistry*, 280(17):17109–17, apr 2005. ISSN 0021-9258. doi: 10.1074/jbc.M414704200.
41. Caitlin E. Tolbert, Peter M. Thompson, Richard Superfine, Keith Burridge, and Sharon L. Campbell. Phosphorylation at Y1065 in Vinculin Mediates Actin Bundling, Cell Spreading, and Mechanical Responses to Force. *Biochemistry*, 53(34):5526–5536, sep 2014. ISSN 0006-2960. doi: 10.1021/bi500678x.
42. Katharina Austen, Pia Ringer, Alexander Mehlich, Anna Chrostek-Grashoff, Carleen Kluger, Christoph Klingner, Benedikt Sabass, Roy Zent, Matthias Rief, and Carsten Grashoff. Extracellular rigidity sensing by talin isoform-specific mechanical linkages. *Nature cell biology*, nov 2015. ISSN 1476-4679. doi: 10.1038/ncb3268.
43. Pia Ringer, Andreas Weißl, Anna-Lena Cost, Andrea Freikamp, Benedikt Sabass, Alexander Mehlich, Marc Tramier, Matthias Rief, and Carsten Grashoff. Multiplexing molecular tension sensors reveals piconewton force gradient across talin-1. *Nature Methods*, 14(11): 1090–1096, sep 2017. ISSN 1548-7091. doi: 10.1038/nmeth.4431.
44. Zengzhen Liu, Philippe Bun, Nicolas Audugé, Maïté Coppey-Moisan, and Nicolas Borghi. Vinculin head-tail interaction defines multiple early mechanisms for cell substrate rigidity sensing. *Integrative biology*, 8(6):693–703, may 2016. ISSN 1757-9708. doi: 10.1039/c5ib00307e.
45. Daniel M Cohen, Brett Kutscher, Hui Chen, Douglas B Murphy, and Susan W Craig. A Conformational Switch in Vinculin Drives Formation and Dynamics of a Talin-Vinculin Complex at Focal Adhesions. *Journal of Biological Chemistry*, 281(23):16006–16015, jun 2006.
46. D. W. Dumbauld, T. T. Lee, A. Singh, J. Scrimgeour, C. A. Gersbach, E. A. Zamir, J. Fu, C. S.

Chen, J. E. Curtis, S. W. Craig, and A. J. Garcia. How vinculin regulates force transmission. *Proceedings of the National Academy of Sciences*, 110(24):9788–9793, may 2013. ISSN 0027-8424. doi: 10.1073/pnas.1216209110.

47. Tomohiro Omachi, Takafumi Ichikawa, Yasuhisa Kimura, Kazumitsu Ueda, and Noriyuki Kioka. Vinculin association with actin cytoskeleton is necessary for stiffness-dependent regulation of vinculin behavior. *PLOS ONE*, 12(4):e0175324, apr 2017. ISSN 1932-6203. doi: 10.1371/journal.pone.0175324.
48. Dapeng Bi, J. H. Lopez, J. M. Schwarz, and M. Lisa Manning. A density-independent rigidity transition in biological tissues. *Nature Physics*, 11(12):1074–1079, dec 2015. ISSN 1745-2473. doi: 10.1038/nphys3471.
49. Benoit B. Mandelbrot and John W. Van Ness. Fractional Brownian Motions, Fractional Noises and Applications. *SIAM Review*, 10(4):422–437, oct 1968. ISSN 0036-1445. doi: 10.1137/1010093.
50. Christopher T Capaldo and Ian G Macara. Depletion of E-Cadherin Disrupts Establishment but Not Maintenance of Cell Junctions in Madin-Darby Canine Kidney Epithelial Cells. *Molecular Biology of the Cell*, 18(1):189–200, jan 2007.
51. Christopher L Tinkle, H Amalia Pasolli, Nicole Stokes, and Elaine Fuchs. New insights into cadherin function in epidermal sheet formation and maintenance of tissue integrity. *Proceedings of the National Academy of Sciences*, 105(40):15405–15410, oct 2008.
52. Judith A. Tunggal, Iris Helfrich, Annika Schmitz, Heinz Schwarz, Dorothee Günzel, Michael Fromm, Rolf Kemler, Thomas Krieg, and Carien M. Niessen. E-cadherin is essential for in vivo epidermal barrier function by regulating tight junctions. *The EMBO Journal*, 24(6): 1146–1156, mar 2005. ISSN 1460-2075. doi: 10.1038/SJ.EMBOJ.7600605.
53. Elsa Bazellières, Vito Conte, Alberto Elosegui-Artola, Xavier Serra-Picamal, María Bintanel-Morcillo, Pere Roca-Cusachs, José J. Muñoz, Marta Sales-Pardo, Roger Guimerà, and Xavier Trepat. Control of cell–cell forces and collective cell dynamics by the intercellular adhesome. *Nature Cell Biology*, 17(4):409–420, apr 2015. ISSN 1465-7392. doi: 10.1038/ncb3135.
54. Tams Vicsek, Andrs Czirk, Eshel Ben-Jacob, Inon Cohen, and Ofer Shochet. Novel type of phase transition in a system of self-driven particles. *Physical Review Letters*, 75(6):1226–1229, aug 1995. ISSN 00319007. doi: 10.1103/PhysRevLett.75.1226.
55. Joanne M Leerberg, Guillermo A Gomez, Suzie Verma, Elliott J Moussa, Selwin K Wu, Rashmi Priya, Brenton D Hoffman, Carsten Grashoff, Martin A Schwartz, and Alpha S Yap. Tension-Sensitive Actin Assembly Supports Contractility at the Epithelial Zonula Adherens. *Current biology : CB*, jul 2014. ISSN 1879-0445. doi: 10.1016/j.cub.2014.06.028.
56. L. Petitjean, M. Reffay, E. Grasland-Mongrain, M. Poujade, B. Ladoux, A. Buguin, and P. Silberzan. Velocity Fields in a Collectively Migrating Epithelium. *Biophysical Journal*, 98(9): 1790–1800, may 2010. doi: 10.1016/j.bpj.2010.01.030.
57. Charlène Gayrard, Clément Bernaudin, Théophile Déjardin, Cynthia Seiler, and Nicolas Borghi. Src- and confinement-dependent FAK activation causes E-cadherin relaxation and β-catenin activity. *The Journal of cell biology*, 217(3):1063–1077, mar 2018. ISSN 1540-8140. doi: 10.1083/jcb.201706013.
58. Katheryn E. Rothenberg, Shane S. Neibart, Andrew S. LaCroix, and Brenton D. Hoffman. Controlling Cell Geometry Affects the Spatial Distribution of Load Across Vinculin. *Cellular and Molecular Bioengineering*, 8(3):364–382, sep 2015. ISSN 1865-5025. doi: 10.1007/s12195-015-0404-9.
59. Paolo Maiuri, Jean-François Rupprecht, Stefan Wieser, Verena Ruprecht, Olivier Bénichou, Nicolas Carpi, Mathieu Coppey, Simon De Beco, Nir Gov, Carl-Philipp Heisenberg, Carolina Lage Crespo, Franziska Lautenschlaeger, Maël Le Berre, Ana-Maria Lennon-Dumenil, Matthew Raab, Hawa-Racine Thiam, Matthieu Piel, Michael Sixt, and Raphaël Voituriez. Actin flows mediate a universal coupling between cell speed and cell persistence. *Cell*, 161 (2):374–86, apr 2015. ISSN 1097-4172. doi: 10.1016/j.cell.2015.01.056.
60. Yasmine Meroz and Igor M. Sokolov. A toolbox for determining subdiffusive mechanisms. *Physics Reports*, 573:1–29, apr 2015. ISSN 03701573. doi: 10.1016/j.physrep.2015.01.002.
61. Silke Henkes, Kaja Kostanjevec, J. Martin Collinson, Rastko Sknepnek, and Eric Bertin. Dense active matter model of motion patterns in confluent cell monolayers. *Nature Communications 2020 11:1*, 11(1):1–9, mar 2020. ISSN 2041-1723. doi: 10.1038/s41467-020-15164-5.
62. Hugues Chaté, Francesco Ginelli, Guillaume Grégoire, and Franck Raynaud. Collective motion of self-propelled particles interacting without cohesion. *Physical Review E - Statistical, Nonlinear, and Soft Matter Physics*, 77(4):046113, apr 2008. ISSN 15393755. doi: 10.1103/PHYSREVE.77.046113/FIGURES/21/MEDIUM.
63. Jin Ah Park, Jae Hun Kim, Dapeng Bi, Jennifer A. Mitchel, Nader Taheri Qazvini, Kelan Tantisira, Chan Young Park, Maureen McGill, Sae Hoon Kim, Bomi Gweon, Jacob Notbohm, Robert Steward, Stephanie Burger, Scott H. Randell, Alvin T. Kho, Dhananjay T. Tambe, Corey Hardin, Stephanie A. Shore, Elliot Israel, David A. Weitz, Daniel J. Tschumperlin, Elizabeth P. Henske, Scott T. Weiss, M. Lisa Manning, James P. Butler, Jeffrey M. Drazen, and Jeffrey J. Fredberg. Unjamming and cell shape in the asthmatic airway epithelium. *Nature Materials*, 14(10):1040–1048, oct 2015. ISSN 14764660. doi: 10.1038/nmat4357.
64. Chiara Malinverno, Salvatore Corallino, Fabio Giavazzi, Martin Bergert, Qingsen Li, Marco Leoni, Andrea Disanza, Emanuela Frittoli, Amanda Oldani, Emanuele Martini, Tobias Lendenmann, Gianluca Deflorian, Galina V. Beznoussenko, Dimos Poulikakos, Kok Haur Ong, Marina Uroz, Xavier Trepat, Dario Parazzoli, Paolo Maiuri, Weimiao Yu, Aldo Ferrari, Roberto Cerbino, and Giorgio Scita. Endocytic reawakening of motility in jammed epithelia. *Nature Materials*, 16(5):587–596, may 2017. ISSN 14764660. doi: 10.1038/nmat4848.
65. Raimon Sunyer, Vito Conte, Jorge Escribano, Alberto Elosegui-Artola, Anna Labernadie, Léo Valon, Daniel Navajas, José Manuel García-Aznar, José J Muñoz, Pere Roca-Cusachs, and Xavier Trepat. Collective cell durotaxis emerges from long-range intercellular force transmission. *Science (New York, N.Y.)*, 353(6304):1157–61, sep 2016. ISSN 1095-9203. doi: 10.1126/science.aaf7119.
66. Eric Theveneau, Lorena Marchant, Sei Kuriyama, Mazhar Gull, Barbara Moepps, Maddy Parsons, and Roberto Mayor. Collective Chemotaxis Requires Contact-Dependent Cell Polarity. *Developmental Cell*, 19(1):39–53, jul 2010. ISSN 1534-5807. doi: 10.1016/J.DEVCEL.2010.06.012.

Materials and Methods

Cells. MDCK type II G cells were maintained in low glucose DMEM with phenol red supplemented with 10% v/v Fetal Bovine Serum (FBS) and Penicillin 10 U/mL + Streptomycin 10 µg/mL, and hTERT RPE-1 cells in DMEM/F12 with 10% v/v FBS, at 37°C and 5% CO2. Cells were transfected with Turbofect transfection reagent (Thermo Scientific) according to the manufacturer's instructions in a WT background to avoid intermolecular FRET between exogenous constructs. 24 hours post-transfection, cells were cultured under drug selection (G418 sulfate 200 µg/mL) for 15 days and FACSed for intermediate expression to avoid level-dependent ectopic localization of exogenous constructs. The generated stable lines were cultured under drug selection. Vinculin auto-inhibition and the natural occurrence of competing isoforms explains how mutant constructs may have a dominant effect without the need for overexpression. The α-catenin KD cell line was a kind gift from the laboratory of W. James Nelson (Stanford U.) (1). The E-cadherin KO cell line was a kind gift from the laboratory of B. Ladoux and R. M. Mège (Institut Jacques Monod) (2). The RPE-1 cell line was a king gift from the laboratory of K. Schauer (Institut Gustave Roussy). Cells were imaged at 37°C and 5% CO2 in Fluorobrite medium supplemented with 10% v/v FBS, Penicillin 10 U/mL + Streptomycin 10 µg/mL, 2.5 mM L-Glutamine and 20mM HEPES on 1.0 borosilicate, 18 or 32mm Ø round glass coverslips or on 2- or 4-well Nunc™ Lab-Tek™ Chambered Coverglass supports (Thermo Scientific) previously coated with collagen IV by incubation with a solution (50 µg/mL in 0.5M acetic acid) of collagen from human placenta Bornstein and Traub Type IV (Sigma) for 10 minutes before air-drying.

Plasmids. VinculinTS (addgene #26019) and Tailless VinculinTS (#26020) were a kind gift of the laboratory of Carsten Grashoff (Westfälische Wilhelms-Universität Münster) (3). The following mutations were introduced with the QuikChange II XL Site-Directed Mutagenesis Kit (Agilent Technologies):
T12 (5'-GAGGTGGCCAAGCAATGTACTGTCGCAGCCA
TTGCAACAAACCTC-3', 5'-CTCACAGACCTGTAAGA
GGTTTGTTGCAATGGCTGCAGCAGTACA-3'),
Y1065E (5'-ATCTGCAGAATTCTTACTGCTCCCATGGG
GTCTTTCTGACC-3', 5'-GGTCAGAAAGACCCCATGG
GAGCAGTAAGAATTCTGCAGAT-3'),

Migration assays. For single cell migration, 36 hours before imaging, cells were passaged at a 1:10 dilution with vigorous pipetting, then 4 to 6 hours before imaging cells were detached once again, resuspended with vigorous pipetting and plated at about 6 cells/mm². For collective migration, 24 hrs before imaging, cells were resuspended and plated at about 600 cells/mm². For biased collective migration, cells were additionally incubated at 37°C in DPBS for 5 to 10 minutes before imaging to weaken calcium-dependent cell-cell contacts and a straight-lined scratch was made in the monolayer using a 200 µL pipette tip. DPBS was then replaced with imaging medium. Prior to imaging, nuclei were stained by incubation in Hoechst 0.1 µg/µl (Thermo Scientific) imaging medium for 20 minutes followed by further dilution to 0.05 µg/µl. Imaging was performed on a ZEISS Axio Observer Z1 widefield microscope with 20x Plan-Apochromat/0.8 dry objective. Hoechst fluorescence was imaged by excitation with a CoolLED pE-300 UV fluorescent lamp, excitation and emission filters 335-383 and 420-470, and an ORCA-Flash4.0 LT camera. Multi-position and multi-tile images were acquired every 10 minutes overnight.

Migration analyses. Nuclear staining detection, cell segmentation and track generation were performed with Imaris 9.2 for single cell migration and Fiji with custom scripts based on Stardist and TrackMate plugins (4, 5) for collective and biased collective migration. Visual inspection of tracks against raw movies enabled manual correction if necessary. Further data analyses were performed with Matlab with custom scripts and @msdanalyser (6).
Apparent cell speed is defined as the distance travelled during the smallest time interval (10min) and directly obtained from cell tracking in Imaris and TrackMate. Speed is averaged over each track, then over the cell population for single cells migration experiments. Speed is averaged over each field of view for each timepoint and over the duration of the experiment for collective and biased collective migration.
Mean square displacement (MSD) is: $\mathrm{MSD}(\Delta t) = \langle(\Delta\mathbf{r}_i(\Delta t))^2\rangle = \langle(\mathbf{r}_i(t+\Delta t) - \mathbf{r}_i(t))^2\rangle$, where $\mathbf{r}_i$ is the position of the cell i at time t and $\langle\rangle$ is the average for all cells and t. For each experiment comprising multiple field of view acquisitions, a weighed mean MSD was calculated to correct for differences in track duration. For each cell line and condition the average MSD was calculated as a weighed mean between experimental replicates to account for potential differences in experiment duration. MSD(Δt) curves were fit with the Fürth equation $\mathrm{MSD} = 4D(\Delta t - P(1-\exp-\Delta t/P))$ where D is the coefficient of diffusion and P the persistence time, or with a straight line in $\ln-\ln$ scale where the slope α is the anomalous exponent.
Step length $R_{i,t}(\Delta t)$ of a cell i is $\sqrt{(\mathbf{r}_i(t+\Delta t) - \mathbf{r}_i(t))^2}$. Step lengths cumulative distributions are displayed for all cells at every time point. Curves from all cells and all time points were fit together with the cumulative distribution function of the Rayleigh distribution $\mathrm{P}(<R) = 1-\exp-R^2/2\sigma^2$ where σ is the scale parameter.
Angular memory $M_{i,t}(\Delta t)$ is defined as the cosine of the angle $\theta_{i,t}$ between the displacement vectors $\mathbf{L}_{i,t}(10\mathrm{min})$ between times t and $t+10$min, and $\mathbf{L}_{i,t-\Delta t}(\Delta t)$ between times $t-\Delta t$ and t of a cell i at time t: $M_{i,t}(\Delta t) = \cos\theta_{i,t}(\Delta t) =$

$\cos(\mathbf{L}_{i,t}^{t+10\text{min}}, \mathbf{L}_{i,t-\Delta t}^{t})$. Figures display $\langle M_{i,t}(\Delta t)\rangle$. This metric measures the duration of the past that the cell considers when deciding on its direction.
Cell shape index is defined as $q = p/\sqrt{A}$, where p and A are the perimeters and areas of the cells approximated by a Voronoi tessellation around nucleus centers, as done previously (7).
Coordination is defined as the cosine of the angle γ between the apparent velocities of cell pairs distant of d.
Directionality is defined as the cosine of the angle ϕ between the cell apparent velocity vector and the direction orthogonal to the wound. Figures display the population average and standard error. Curves were fit with a one-phase association equation: $\cos\phi = \cos\phi_{\text{max}}(1-\exp(-t/\tau_{\text{d}}))$ where $\cos\phi_{\text{max}}$ is the average directionality at the infinite time limit and τ_{d} the characteristic time to reach it.
Wound closure speed is defined as the rate of wound half-area $A/2$ decrease in $\Delta t = 30$min normalized to wound length l: $\text{WC} = (A(t+\Delta t) - A(t))/2l\Delta t$.

Simulations. Self Propelled Particles (SPP) simulations were performed in R software (version 4.2.2) on $N = 200$ particles within a 2D square box of side L with periodic boundary conditions for $T = 600$ steps of duration τ. From an initial condition of random positions and orientations of all particles, the position of each particle i is updated according to $\mathbf{r}_i(t+\tau) = \mathbf{r}_i(t) + \mathbf{v}_i(t+\tau)\tau$, where $\mathbf{v}_i$ is the velocity of particle i with constant modulus v and an orientation $\theta_i(t+\tau) = \arg\left[\sum_{j,|\mathbf{r}_i(t)-\mathbf{r}_j(t)|<d}\mathbf{v}_j(t)\right] + \eta\xi_i$. The first term accounts for an interaction that causes velocity alignment between neighbors within a distance d (8). The second term is a white noise $\xi_i(t)$ over $[-\pi,\pi]$ bounded by $\eta \in [0,1]$, which defines the directional freedom of an isolated particle. The intrinsic cell persistence, i.e. that of an isolated cell, directly relates to η and τ through $P_0 = \tau(\overline{\cos\theta_i})^{1/2}/(1-\overline{\cos\theta_i})$ where $\overline{\cos\theta_i} = \sin\eta\pi/(\eta\pi)$, by generalization of Fürth's approach (9) to two dimensions. The apparent speed $v = 2.5$µm.min^{-1} was fixed in the typical range of experimental measurements. The total particle density $\rho = N/L$ was set to various values within $[10^{-5}, 10^{-2}]$cell.µm^{-2} to match single ($\rho \ll 10^{-3}$cell.µm^{-2}) or collective ($\rho \geq 10^{-3}$cell.µm^{-2}) cell migration assays. The interaction distance $d = 5-40$µm was varied around the cell size scale. The directional freedom η was varied within $]0,1[$ for the sake of exhaustiveness. Simulated tracks were analysed as live cell tracks to compute the $MSD(\Delta t)$ that was fitted in ln-ln scale with the minpack.lm R package. Fit parameters P and α were averaged over 5 simulations for each combination of parameter values and linearly interpolated on a 400x400 grid between extreme values of P_0/τ and $\pi\rho d^2$ for representation purposes. The $P-\alpha$ boundary was set at the transition in majority behavior within moving boxes of size 0.25 in log-log scale.

Confocal and molecular tension microscopy. Cells were imaged on a ZEISS LSM780 confocal microscope with a 63x/1.4NA oil immersion objective. The mTFP1 donor fluorophore was excited by a 458 nm Argon laser line. Fluorescence emission was detected in the 473nm-561nm spectrum with a spectral resolution of 8.8nm (10 channels) by a GaAsP (Gallium Arsenide Phosphide) detector. The pixel resolution was 0.086µm. Z-stacks step was 367 nm. Image analysis was performed in Fiji. Segmentation of FAs for FRET index measurements was performed by a custom macro that subtracts the background, applies a Gaussian filter, thresholds, localizes particles of an area of 0.7 µm² or more and a circularity factor between 0 and 0.95 and displays the final Region Of Interest (ROI) set with the HiLo look up table to enable manual removal of any spurious or saturated ROI. Segmentation of AJs was performed manually. FRET index = FRET/(Donor+FRET) is calculated using the PixFRET plugin in Fiji (10) from the channels around 494 and 530nm (Donor and FRET channels respectively) of the spectral stack, a 2px radius Gaussian filter and a threshold above 1x mean background intensity. Using the ROI set generated from the corresponding intensity image, the ROI pixels belonging to one cell are combined to obtain an average FRET index value of FAs or AJs per cell.

Fluorescence recovery after photobleaching. FRAP was performed on a Yokogawa Spinning Disk CSU-X1 microscope. Cells were imaged with a 63x/1.4NA oil immersion objective. Fluorescence was acquired by 491nm laser excitation with a GFP 525/50 emission filter and a sCMOS PRIME 95 camera (Teledyne-Photometrics). Photobleaching was achieved by a 476nm FRAP laser. Images were analyzed with ImageJ. Fluorescence in ROIs was background-subtracted, corrected for photobleaching due to imaging and normalized by the fluorescence before photobleaching. The lack of contrast between photobleached adhesion structures and their surrounding at $t = 0$ ensured 100% photobleaching. The average curves for each condition were then fitted with a two-phase association equation: $F = F_{\text{fast}}(1-\exp(-t/\tau_{\text{fast}})) + F_{\text{slow}}(1-\exp(-t/\tau_{\text{slow}}))$ where F_{fast} is the fluorescence of the mobile fraction characterized by the time τ_{fast} that accounts for the very fast initial recovery and F_{slow} the fluorescence of the mobile fraction characterized by the time τ_{slow} that accounts for the second recovery phase. The immobile fraction is therefore $1 - F_{\text{fast}} - F_{\text{slow}}$.

Western Blot. Cells were washed with PBS at 4°C, lysed on ice in RIPA buffer (with protease and phosphatase inhibitors) by scraping, collected in centrifugation tubes, vortexed for 1 minute and centrifuged at 13000 rpm for 15 minutes at 4°C. Supernatant was then collected and diluted with an equal volume of Laemmli Buffer 2x (Sigma). Samples were loaded on a Mini-Protean TGX Precast gel (BioRad), ran for 1 hour at 100 V in running buffer (Tris-Glycine buffer 1x, SDS 0.005%) and

transferred onto a nitrocellulose membrane in a 10% methanol transfer buffer (Tris-Glycine 1x, methanol 10%) for 1 hour at 100 V. The transfer was verified by staining with Ponceau S solution. The membrane was blocked for 30 minutes at room temperature in a 5% milk in TBST solution (Tris-buffer saline solution 1X, 0.05% Tween 20) followed by overnight incubation with the mouse anti-Vinculin V-9131 (Sigma) primary antibody in 5% milk in TBST solution. The membrane was then washed three times with TBST solution for 5 minutes each time and incubated for 1 hour at room temperature with HRP-Goat anti-Mouse (Invitrogen 626520) secondary antibody in 5% milk in TBST solution. Prior to revelation the membrane was once again washed three times with TBST solution for 5 minutes each time. Signal was developed using SuperSignal® West Femto Maximum Sensitivity Substrate Kit (Thermo Scientific) according to the manufacturer's instruction and a ChemiDoc™ MP Imaging system (BioRad).

Statistical analysis. Statistical analyses were performed mainly using the GraphPad Prism VII or R software. Data is represented with mean $\pm$ SEM unless stated otherwise. Data were pooled between independent experiments whenever the variability between statistical units within an experiment accounted for the total variability. Differences between conditions were assessed with the non-parametric, unpaired, two-tailed Mann-Whitney test. Linear regressions by the least-squares method were tested against the null hypothesis slope=0 using an extra sum-of-squares F test. FRAP fits by the least-squares method were compared using an extra sum-of-squares F test with shared immobile fraction between FL and each mutant as the null hypothesis. Correlations were calculated using the Pearson correlation. MSD models were compared using the score $1/(\exp \Delta\mathrm{AIC} + 1)$ where AIC is the Akaike Information Criterion. *: p<0.05, **: p<0.01, ***: p<0.001, ****: p<0.0001.

Supplementary References

1. Jacqueline M Benjamin, Adam V Kwiatkowski, Changsong Yang, Farida Korobova, Sabine Pokutta, Tatyana Svitkina, William I Weis, and W James Nelson. Alpha-E-catenin regulates actin dynamics independently of cadherin-mediated cell–cell adhesion. *Journal Of Cell Biology*, 189(2):339–352, 2010. doi: 10.1083/jcb.200910041.
2. Lakshmi Balasubramaniam, Amin Doostmohammadi, Thuan Beng Saw, Gautham Hari Narayana Sankara Narayana, Romain Mueller, Tien Dang, Minnah Thomas, Shafali Gupta, Surabhi Sonam, Alpha S. Yap, Yusuke Toyama, René-Marc Mège, Julia M. Yeomans, and Benoît Ladoux. Investigating the nature of active forces in tissues reveals how contractile cells can form extensile monolayers. *Nature Materials 2021 20:8*, 20(8):1156–1166, feb 2021. ISSN 1476-4660. doi: 10.1038/s41563-021-00919-2.
3. Carsten Grashoff, B.D. Hoffman, M.D. Brenner, Ruobo Zhou, Maddy Parsons, M.T. Yang, M.A. McLean, S.G. Sligar, C.S. Chen, Taekjip Ha, and Others. Measuring mechanical tension across vinculin reveals regulation of focal adhesion dynamics. *Nature*, 466(7303):263–266, 2010. doi: 10.1038/nature09198.
4. Jean Yves Tinevez, Nick Perry, Johannes Schindelin, Genevieve M. Hoopes, Gregory D. Reynolds, Emmanuel Laplantine, Sebastian Y. Bednarek, Spencer L. Shorte, and Kevin W. Eliceiri. TrackMate: An open and extensible platform for single-particle tracking. *Methods*, 115:80–90, feb 2017. ISSN 1046-2023. doi: 10.1016/J.YMETH.2016.09.016.
5. Uwe Schmidt, Martin Weigert, Coleman Broaddus, and Gene Myers. Cell detection with star-convex polygons. *Lecture Notes in Computer Science (including subseries Lecture Notes in Artificial Intelligence and Lecture Notes in Bioinformatics)*, 11071 LNCS:265–273, 2018. ISSN 16113349. doi: 10.1007/978-3-030-00934-2_30/TABLES/1.
6. Nadine Tarantino, Jean Yves Tinevez, Elizabeth Faris Crowell, Bertrand Boisson, Ricardo Henriques, Musa Mhlanga, Fabrice Agou, Alain Israël, and Emmanuel Laplantine. Tnf and il-1 exhibit distinct ubiquitin requirements for inducing NEMO-IKK supramolecular structures. *Journal of Cell Biology*, 204(2):231–245, jan 2014. ISSN 00219525. doi: 10.1083/JCB.201307172/VIDEO-7.
7. Kevin Suh, Youn Kyoung Cho, Isaac B. Breinyn, and Daniel J. Cohen. E-cadherin biomaterials reprogram collective cell migration and cell cycling by forcing homeostatic conditions. *Cell Reports*, 43(2), feb 2024. ISSN 22111247. doi: 10.1016/j.celrep.2024.113743.
8. Tams Vicsek, Andrs Czirk, Eshel Ben-Jacob, Inon Cohen, and Ofer Shochet. Novel type of phase transition in a system of self-driven particles. *Physical Review Letters*, 75(6):1226–1229, aug 1995. ISSN 00319007. doi: 10.1103/PhysRevLett.75.1226.
9. Reinholdrth Fürth. Die Brownsche Bewegung bei Berücksichtigung einer Persistenz der Bewegungsrichtung. Mit Anwendungen auf die Bewegung lebender Infusorien. *Zeitschrift für Physik*, 2(3): 244–256, jun 1920. ISSN 14346001. doi: 10.1007/BF01328731.
10. Jérôme N Feige, Daniel Sage, Walter Wahli, Béatrice Desvergne, and Laurent Gelman. PixFRET, an ImageJ plug-in for FRET calculation that can accommodate variations in spectral bleed-throughs. *Microscopy research and technique*, 68(1):51–8, sep 2005. ISSN 1059-910X. doi: 10.1002/jemt.20215.

Table 1. Most likely walk model for single cell migration

Cells	Relative likelihood of persistent diffusion vs. pure or super-diffusion
WT	>0.9999
FL	>0.9999
TL	>0.9999
T12	>0.9999
YE	>0.9999
RPE-1	>0.9999

Table 2. Most likely walk model for collective cell migration

Cells	Relative likelihood of persistent diffusion vs. pure or super-diffusion	Anomalous exponent
WT	$< 10^{-4}$	1.73 ± 0.003
FL	$< 10^{-4}$	1.699 ± 0.008
TL	< 0.4172	1.52 ± 0.01
T12	$< 10^{-4}$	1.545 ± 0.007
YE	$< 10^{-4}$	1.636 ± 0.007
$\alpha-$catenin KD	< 0.1155	1.192 ± 0.009
E-cadherin KO	$< 10^{-4}$	1.847 ± 0.005
RPE-1	$< 10^{-4}$	1.625 ± 0.005

Table 3. Most likely walk model for directed collective cell migration

Cells	Relative likelihood of persistent diffusion vs. pure or super-diffusion	Anomalous exponent
WT	$< 10^{-4}$	1.52 ± 0.01
FL	$< 10^{-4}$	1.718 ± 0.003
TL	$< 10^{-4}$	1.571 ± 0.008
T12	$< 10^{-4}$	1.687 ± 0.006
YE	$< 10^{-4}$	1.55 ± 0.01
$\alpha-$catenin KD	$< 3.10^{-4}$	1.199 ± 0.008
E-cadherin KO	$< 10^{-4}$	1.846 ± 0.004

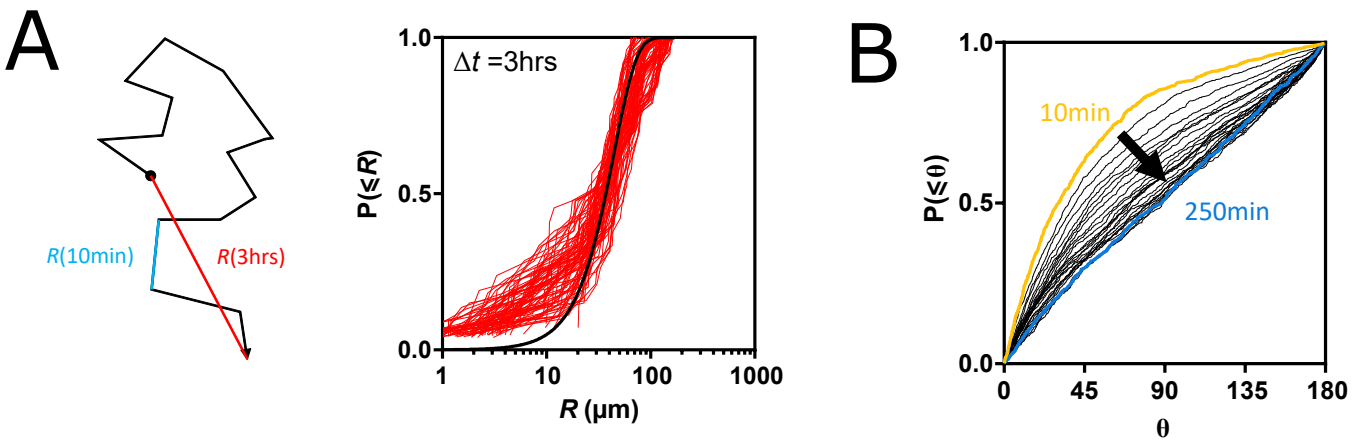

Fig. S 1. (A) Left: Schematic migration track and step length ($R(\Delta t)$, see Materials and Methods) at $\Delta t = 10$min (blue) and $\Delta t = 250$min (red). Right: cumulative distributions of the step length R for $\Delta t = 3$hrs of single cells. One red curve per frame pair along a movie. The black line is a global fit of all red curves with a cumulative Rayleigh distribution function. (B) Cumulative distributions of the angular deviation ($\theta(\Delta t)$, see Materials and Methods) between $\Delta t = 10$min (yellow) and $\Delta t = 250$min (blue) of single cells. Data from 94 cell tracks of 2 independent experiments (same as in Fig. 1).

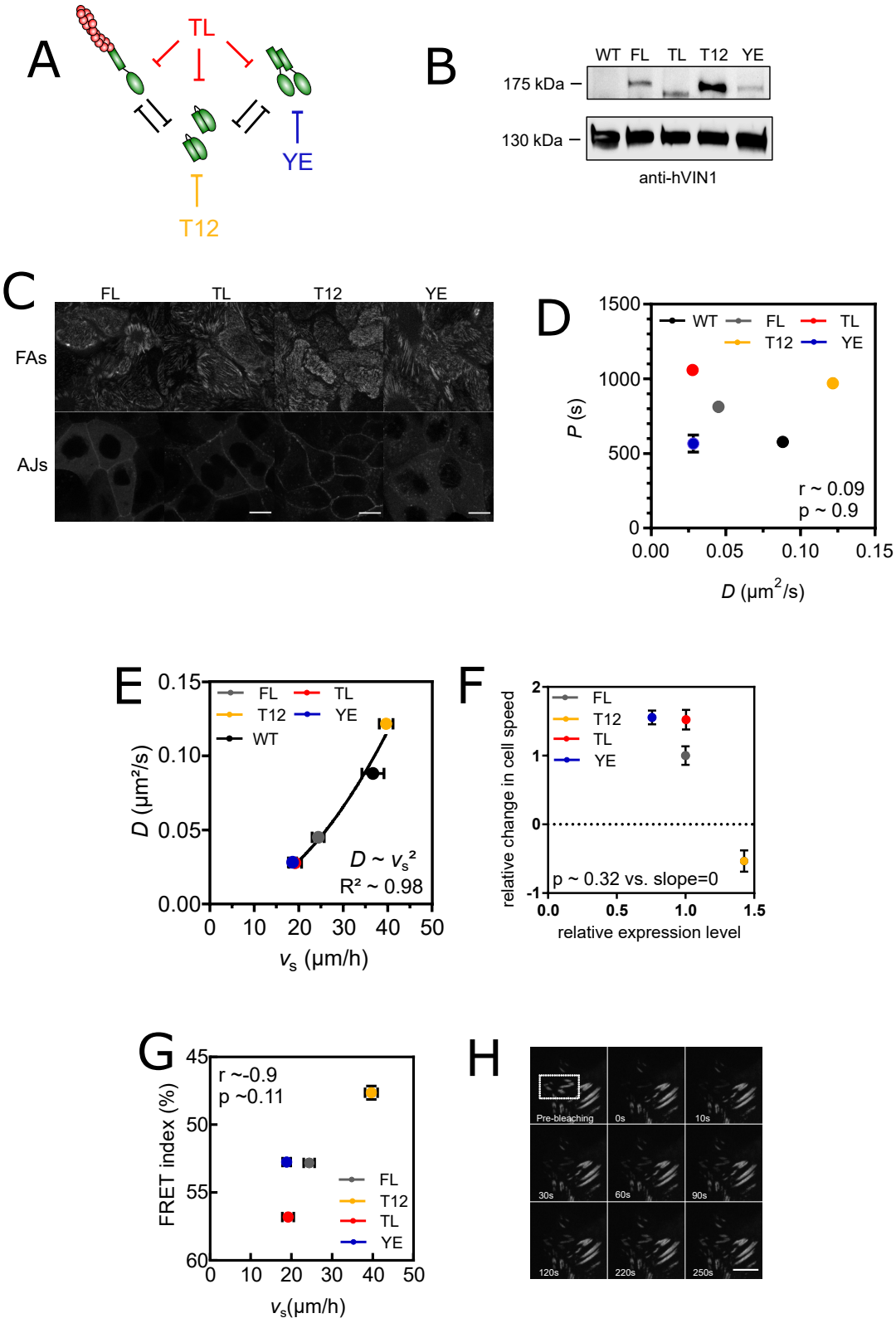

Fig. S 2. (A) Vinculin (green) and the different interactions (head-tail, tail-tail and actin-tail) and mutants (TL, T12 and YE) considered in this study. (B) Western Blot of the WT cells and cells expressing the FL, TL, T12, and YE vinculin TSMod constructs labelled for vinculin (WT at 130kDa, TSMod at 175kDa). (C) Direct fluorescence of the vinculin TSMod constucts in the FAs (top) and AJs (bottom) planes. Scale bar=20μm. (D) Persistence time P as a function of diffusion coefficient D for WT, vinculin FL and mutant single cells. Pearsons correlation coefficient r and p-value. (E) Diffusion coefficient D as a function of the apparent speed v_s of WT, vinculin FL and mutant single cells, globally fit the Fürth equation with $\Delta t = 10$min. (F) Relative change in single cell apparent speed as a function of vinculin FL or mutant expression level. p-value of an extra sum-of-squares F test on a linear regression with slope=0 as the null hypothesis. (G) FRET index as a function of apparent speed v_s for vinculin FL and mutant single cells. Pearsons correlation coefficient r and p-value. (H) Direct fluorescence of vinculin TSMod in FAs during FRAP. White Box shows the FRAPed region. Scale bar=5μm. Data of (D-F) from 94 (WT), 125 (FL), 129 (TL), 193 (T12) and 110 (YE) cell tracks of 2 (WT) and 3 (all others) independent experiments (same as in Figs. 1 and 2A,B). Data of (G) as above for v_s and from 81 (FL), 102 (TL), 52 (T12) and 84 (YE) cells of 4 (FL) and 3 (TL, T12, YE) independent experiments for FRET index (same as in Fig. 2B,D). Mean $\pm$ SEM.

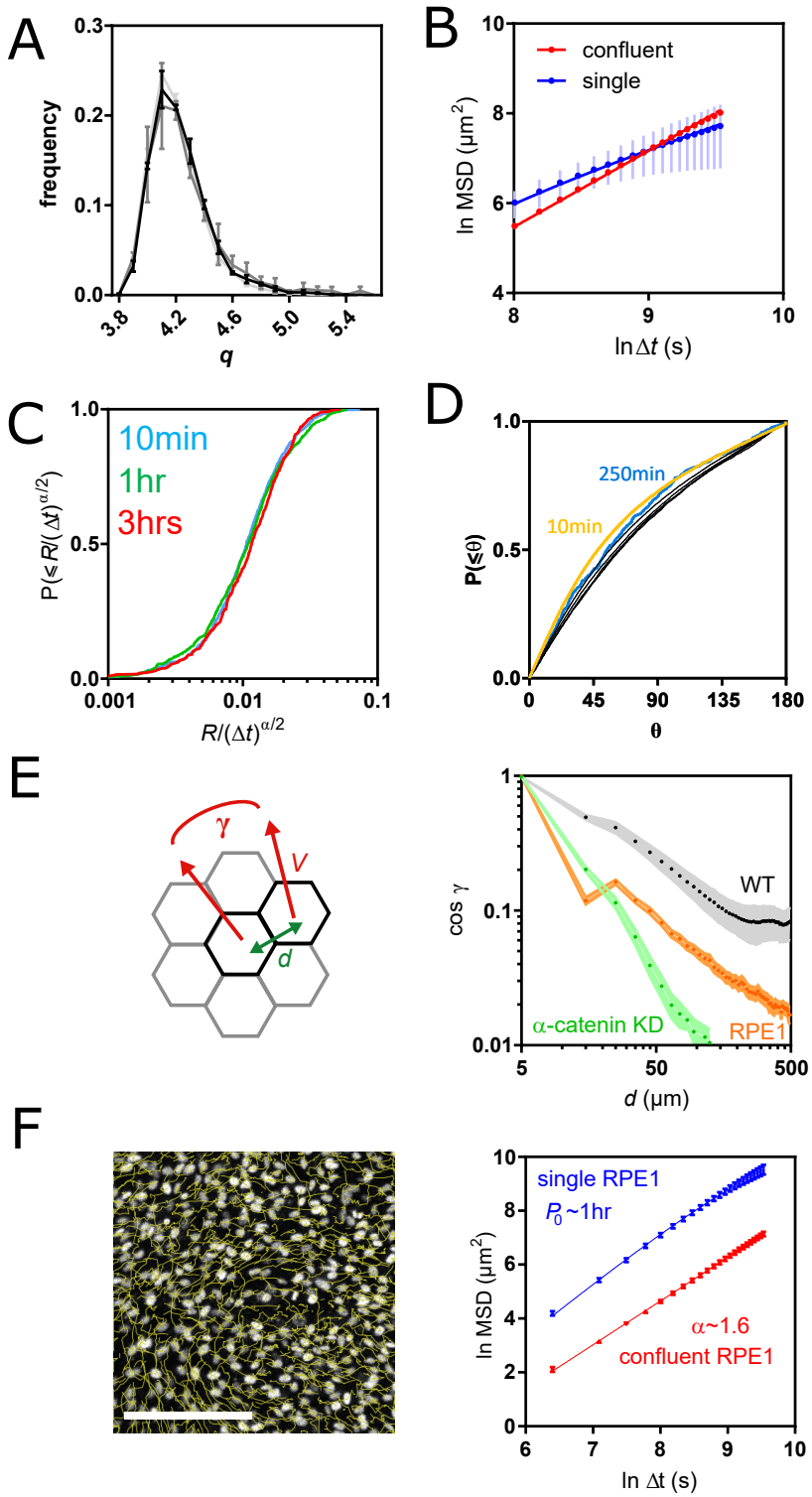

Fig. S 3. (A) Cell shape index index distribution of WT cells at confluence. (B) MSD(Δt) of single (blue) and confluent (red) cells at long time scales. (C) Cumulative distributions of the normalized step length $R/(\Delta t)^{\alpha}$ where α is the anomalous exponent, for $\Delta t = 10$min, 1hr and 3hrs at confluence. One representative frame pair per Δt. (D) Cumulative distributions of the angular deviation $\theta(\Delta t)$, see Materials and Methods) between $\Delta t = 10$min (yellow) and $\Delta t = 250$min (blue) of confluent cells. (E) Average coordination $< \cos\gamma >$ as a function of intercellular distance d in WT and α-catenin cells at confluence. (F) Left: fluorescence image of nucleus-stained RPE-1 cells at confluence and their migration tracks in yellow. Right: MSD(Δt) of single (blue) and confluent (red) RPE-1 cells with best fitting model parameters. Data from (A) 3 and (B-E) 11 (WT) and 4 (α-catenin) FOV (500-1000 tracks each) of 3 independent experiments (same as in Fig. 3B-F). (F) Data from 11 FOV (500-1000 tracks each at confluence) of 2 (single) and 3 (confluent) independent experiments. Scale bar = 100μm. Mean $\pm$ SEM.

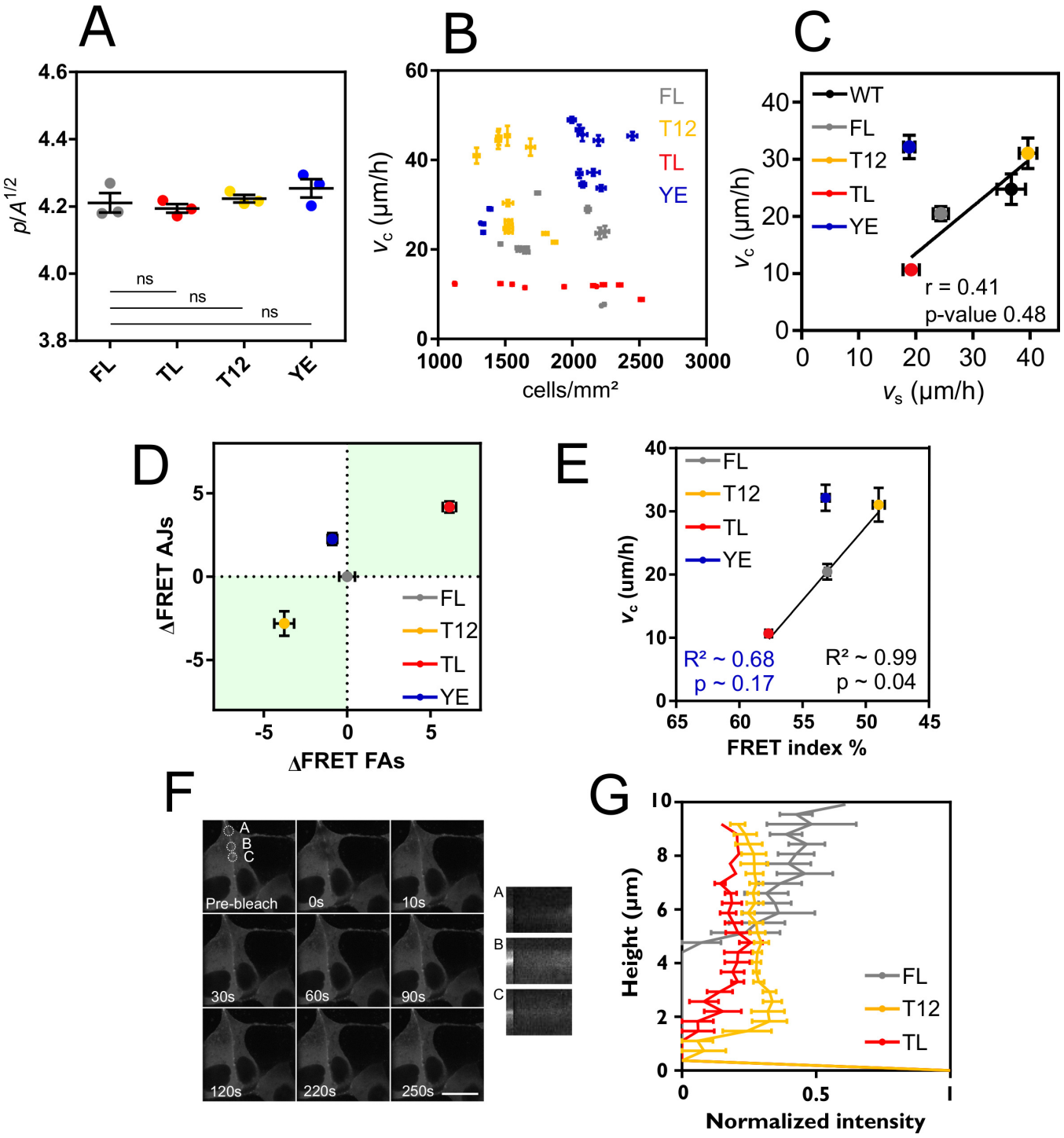

Fig. S 4. (A) Mean cell shape index as a fucntion of vinculin mutant. (B) Apparent collective cell speed (v_c) as a fucntion of cell density per FOV. (C) Apparent collective cell speed (v_c) as a function of apparent single cell speed (v_s) for WT cells and cells expressing the vinculin FL and mutant constructs. Pearson coefficient r and p-value. (D) FRET index of the vinculin mutants relative to vinculin FL at AJs vs. FAs. (E) Apparent collective cell speed (v_c) as a function of FRET index of vinculin constructs. Pearson coefficient R^2 and p-value for all cell lines (blue) and without the YE mutant (black). (F) Left: direct fluorescence of vinculin TSMod in AJs during FRAP. Right: kymographs of the circled, FRAPed regions A, B, C on the left Scale bar=5μm. (G) Lateral recruitment of FL, TL and T12 at AJs as a function of height normalized to FA intensity (5, 6, 7 cells respectively). Data of (A) from 3 independent experiments for each mutant (500-1000 cells each). Data of (B,C) from 94 (WT), 125 (FL), 129 (TL), 193 (T12) and 110 (YE) cell tracks of 2 (WT) and 3 (all others) independent experiments for v_s) (same as in Figs. 1 and 2A,B) and from 11 (WT), 12 (FL), 11 (TL, T12) and 14 (YE) FOV (500-1000 tracks each) of 3 independent experiments for v_c) (same as in Figs. 3B-D and 4A,B). Data of (D) from 169 (FL), 30 (TL) and 64 (T12, YE) contacts of 5 (FL) and 3 (TL, T12, YE) independent experiments for AJs, and from 45 (FL), 35 (TL), 104 (T12) and 67 (YE) cells of 4 (FL) and 3 (TL, T12, YE) independent experiments for FAs (same as in Fig. 4D,E). Data of (E) as in (C) for v_c and in (D, FAs) for FRET index. Mean $\pm$ SEM.

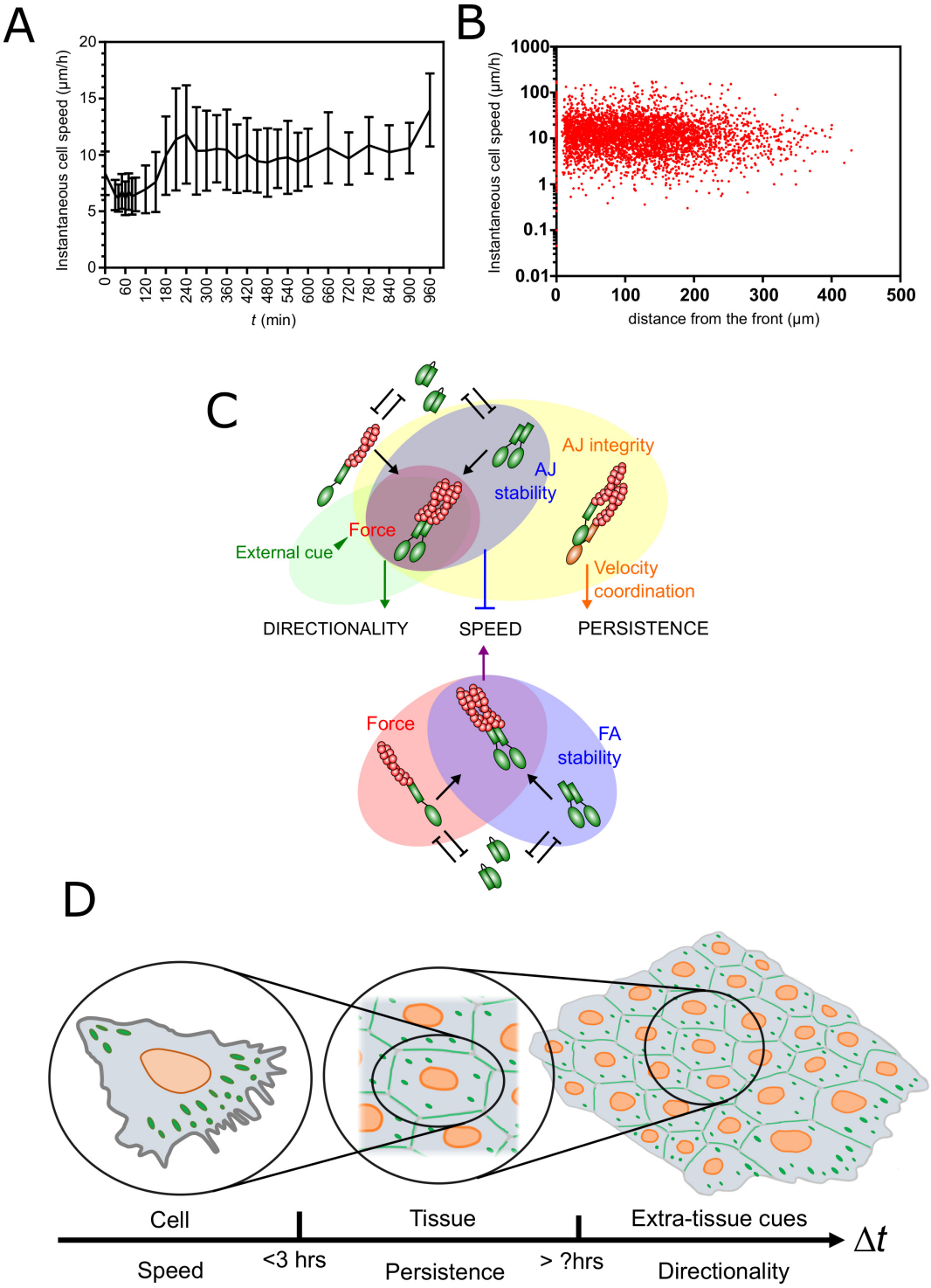

Fig. S 5. (A) Apparent cell speed as a function of time in a wound healing assay. (B) Apparent cell speed as a function of the distance to the front at 6 hours after wounding. (C) Complete model for the control of cell speed persistence and directionality by the stability and force transmission of adhesions, from Fig. 2F, 4G, 6F) (D) Working model for the control of cell spatial exploration efficiency as a function of time scales (see text for details). Data of (A) from 3 FOV (500-1000 tracks each) of 3 independent experiments. Mean ± SEM. Data of (B) from 5 FOV (about 1000 cells each) of 5 independent experiments.